From Knowledge to Wisdom

Journal of Geological Resource and Engineering

Journal of Geological Resource and Engineering

David Publishing Company
www.davidpublisher.com

Contents

Geomorphologic Model of Gunungsewu Karst, Gunung Kidul Regency, Yogyakarta Special Territory, Indonesia: The Role of Lithologic Variation and Geologic Structure

Sari Bahagiarti Kusumayudha, Jatmiko Setiawan, Ayu N. Ciptahening and Prabawa Dwi Septianta

Department of Geology, Universitas Pembangunan Nasional "Veteran" Yogyakarta, Condongcatur, DIY 55283, Indonesia

Abstract: Gunungsewu is a karst terrain that shows unique geomorphologic phenomena. The area is mainly composed of limestone of Wonosari Formation. Interaction of tectonic, erosion, denudation, and deposition occurred since Miocene period brings about diversity of landforms that supporting the development of this area as a natural laboratory, specific interest, scientific and educational tourisms. In general the geomorphology of Gunungsewu can be classified into two groups of landforms, the first is positive relief and the second is negative relief. The positive relief includes hills of conical, dome, convex-cone, convex and ridge. The negative relief involves cave, shaft, doline, uvala, locva and polje. This diversity is influenced by variation of physical properties of rock composing the landforms, such as hardness, internal friction angle, and geologic structures including thickness and position of bedding plane as well as joint pattern.

Key words: Geomorphology, karst, rock properties, geologic structures.

1. Introduction

Gunungsewu is very famous in Indonesia, especially in Java Island, as a karst terrain that is geologically, geomorphologically and hydrogeologically shows unique phenomena. Geology of Gunungsewu expresses tracks of tectonic, erosion, denudation, and deposition occurred since Miocene epoch. These processes brought about morphologic diversities that support for the development of this area as natural laboratory, special interest, scientific, and education tourisms. Therefore Gunungsewu is very potential to be promoted as an international level of geopark [1].

Gunungsewu displays a specific Tropical landform, characterized by the existence of hills, closed depressions, and caves. Although morphology of Gunungsewu area is as an ordinary karst landforms, but there is a diversity. The diversity seems to be reflecting the occurrence of various geologic factors influencing the landform process.

It is interpreted that the morphology is influenced by variation of physical properties of the lithology and the existing geologic structures. This hypothetical view has to be verified. In relation to that, such an assessment is needed to be done. Therefore, this study is aimed to identify geologic factors that role in the formation of karst morphology of the Gunungsewu, and develop a geomorphologic model of this area.

The study area is located in Gunungsewu karst area of Yogyakarta Special Territory, Indonesia, geographically lies of 7°57'-8°14' south latitude, and 110°19'-110°50' east longitude, about 25 km southeastern of Yogyakarta city. Case study was especially taken in the Ponjong and Karangmojo districts, Gunung Kidul Regency, on the coordinate of 468,750 mE-473,750 mE and 9,117,000 mN-9,122,000 mN. Fig. 1 shows the location of the study area that can be reached easily by cars from Yogyakarta city.

Corresponding author: Sari Bahagiarti Kusumayudha, professor, research fields: geology and hydrogeology. E-mail: saribk@upnyk.ac.id.
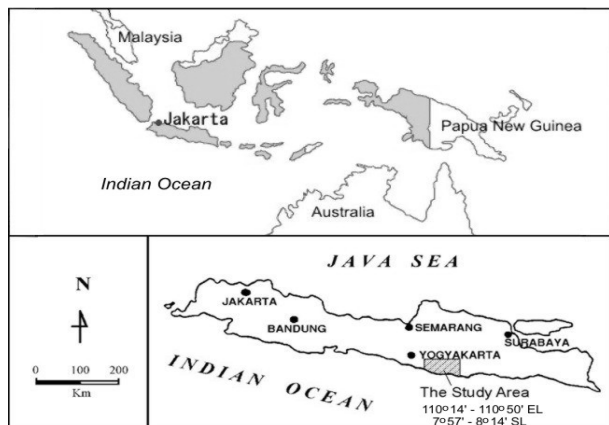
Fig. 1   Map showing the location of the study area.

2. Methods of Study

Approach method applied in the study was field surveying, surface geologic and geomorphologic mapping, topographic interpretation, remote sensing, petrologic and geologic structure assessment. Data used for the analyses were derived from field surveys and mapping, and from existing previous studies. Remote sensing method was run by using airphotoes of 1 : 35,000 scale and satellite images (Ers and Google Earth).

Survey and mapping were done to identify variation physical characteristics and distribution of the lithology. Geologic structure identification and measurements were operated for strike and dip and also shape of karst morphology such as hill, ridge, and valleys. Topographic and image interpretation were utilized for determining pattern and orientation of fracture system (joint, fractures, fault) also hills and valleys lineaments.

3. Geology

Geologic setting of Gunungsewu belongs to western part of Southern Mountains [2]. The stratigraphy from the oldest to the youngest is composed of Semilir formation, Nglanggran formation, Sambipitu formation, Oya formation, Wonosari formation, Kepek formation, and locally Terrarosa deposit.

Semilir formation belongs to deep sea sedimentary rocks consists of sandstone, tuff, tuffaceous sandstone,

lapilli, tuff breccias, lappilli breccias, agglomerate, andesitic breccias, clay stone, siltstone, and shale of Oligocene—Early Miocene [3]. Semilir formation is overlain by Nglanggeran formation, consists of andesitic breccias, agglomerate, polymixed breccias, lava deposits, sandstone and tufaceous sandstone. Age of the formation is oligomiocene to Middle Miocene [3]. Nglanggeran formation is conformably overlain by sambipitu formation that comprises marl, claystone, calcareous siltstone, calcareous sandstone and tuffaceous sandstone. Sambipitu formation is Middle Miocene age [3]. Oya formation conformably overlays Sambipitu formation. This rock unit consists of calcarenite, bedded limestone, calcareous sandstone and tuffaceous-calcareous sandstone. Age of the formation is Middle Miocene to Mio-Pliocene [4]. Oya formation is overlain by Wonosari formation that consists of reef, massive and bedded limestones of Middle Miocene to Pliocene age [4]. Kepek formation consists of marl and calcarenite that lays over the Wonosari formation of Pliocene—Pleistocene epoch [4]. The geologic map of the study area is shown in Fig. 2.

Gunungsewu has been uplifted and a little bit folded since middle miocene or about 6 million years ago [3]. There is a syncline expresses as the Wonosari plateau with axial orientation of N75^{o}E-N255^{o}E, dipping no more than 10°, while the hills display homoclinal dipping 5° to 15° relatively southward [4, 5]. In the Ponjong and Karangmojo areas, dip of the bedding planes reaches 18°.

Patterns of fault, joints, and fissures that is mapped by using Earth Resource Satelite, generally shows northwest-southeast direction [5, 6]. On the other hand, the general dip direction is to southwest, southeast, and south [4, 7], while the joint patterns shows northwest-southeast and northeast-southwest.

4. Karst Geomorphology

There are some requirements to form such a perfect karst, this include the existence of limestone of > 200 m thickness, massive but jointed, and bedded [8]. There

Geomorphologic Model of Gunungsewu Karst, Gunung Kidul Regency, Yogyakarta Special Territory,
Indonesia: The Role of Lithologic Variation and Geologic Structure

3
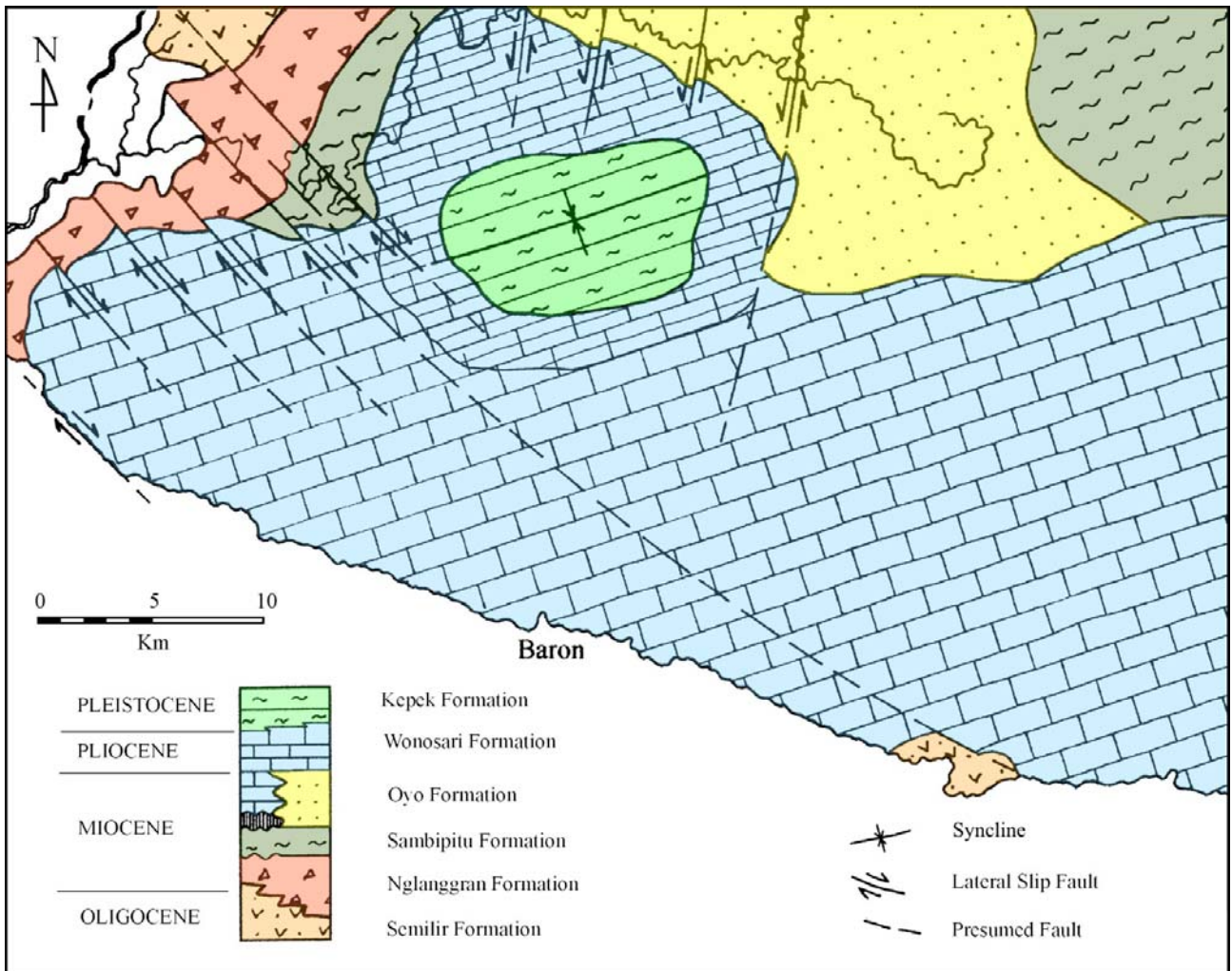
Fig. 2 Geologic map of Gunungsewu area [5, 6].

must be valleys that the elevation is lower than the position of the limestone. Karstification also needs warm climate, high enough rainfall (> 2000 mm/year); and relatively slow tectonic activity (uplifting) involving all of the area [9].

Beside the requirements mentioned above, morphologic diversity of karst is influenced by physical characteristics of the limestone, including strength and hardness [10]. Joints, cracks, faults and bedding planes are factors that contribute in karstification process [11], into which dissolution occurs.

All of the Gunungsewu area spreading is about 1,500 km^2. Based on air photo interpretation, there are more or less 45.000 hills [4], with various shapes, such as cone, dome, convex and ridge (Figs. 3-6). The negative reliefs include doline, uvala, locva, polje, shaft and cave.

Fig. 3 Cone karst.

Fig. 4   Convex cone karst.

Fig. 5   Dome karst.

Fig. 6   Ridge karst.

5. Influence of Lithologic Variation and Geologic Structure

Limestone of Wonosari Formation in the Gunungsewu Area is composed of some lithofacieses,

such as bedded limestone consist of packstone and wackestone, and reef limestone or boundstone [4-6]. Beside wackestone, packstone and boundstone, there is also grainstone [12]. The limestone physically shows karstification or hard and cavernous and calcification (chalky limestone), weak or brittle. If such limestones is uplifted and exposed in the area with wet tropical climate, karstification will happen. But when the limestone is exposed in an arid with a few rainfall condition, calcification will occur [13]. The sequence of caliche consists of hardpan, platty caliche, nodular caliche and chalky caliche. [14].

In this study, result of geomorphologic and geologic mapping on the distribution and variation of lithology and geologic structure verifies that different physical characteristic of lithology forms different shape of morphology, either positive or negative reliefs. In this case, internal friction angle (φ) of limestone has an important role in producing the slope of morphology of the karst. Table 1 contains various values of internal friction angle of limestone from some sources.

The orientation of geologic structures especially joint, fault, and fissures control the lineaments of hills, valleys, that are Northwest-Southeast and Northeast-Southwest [15, 16]. The dip of bedding plane influences morphologic dimension. Table 2 displays orientations of joint patterns and hills or valleys lineaments.

6. Karst Geomorphologic Model of Gunungsewu

Karst geomorphology modeling of the Gunungsewu area, comprises some aspecs including morphographic morphometric, and morphogenesis [17]. Morphogenesis involves passive morphostructure, physical properties of the lithology, active morphostructure

Table 1   Values of internal friction angle (φ) of karstic limestone and caliche [10, 18-20].

Limestone (°)	Dolomite, chalky limestone (°)	Source
33-40	27-31	Hoek & Bray (1981)
35-50	22	Jumikis (1983)
34.8-42	31.5-35.5	Goodman (1989)
32-49	30-41	Franklin & Dussault (1989)

Geomorphologic Model of Gunungsewu Karst, Gunung Kidul Regency, Yogyakarta Special Territory, Indonesia: The Role of Lithologic Variation and Geologic Structure

5

Table 2   Orientations of joint pattern, hills and valleys lineaments.
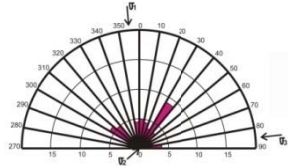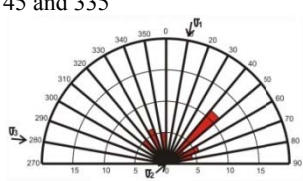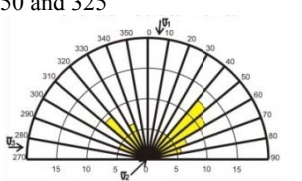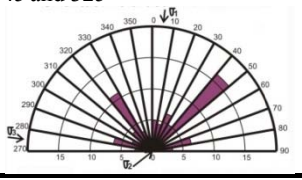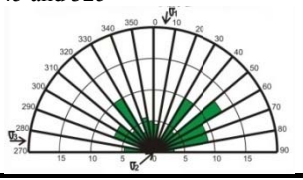
Measured from:	Orientation of the pattern (N…^{o}E)		
	Joint	Hills lineament	Valleys lineament
Field (175 samples)	35 and 315		
Satellite image		45 and 335	50 and 325
Topographic map		45 and 325	45 and 325

Table 3   Model of the influence of lithologic physical properties and geologic structures to positive relief karst morphology.
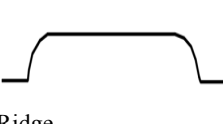
Lithology	Morphology		Morphogenesis		
	Morphographic	Morphometric	Active morphostructure (geologic structures)	Passive morphostructure (physical properties)	Morphodynamic (exogenic processes)
Dominated by bedded limestone, grainstone and packstone	Cone	-Steep slope -Slope: 30°-45° -Relatively top sharp -Height: 30-90 m	-Joint -Thin bedded: < 1 m -Bedding plane inclination: > 5°	hard, cavernous, lapies, φ = 32-50	Karstification
Dominated by reef limestone, boundstone	Convex-cone	-Steep slope -Slope: 35°-45° -Top convex -Height: 30-70 m	-Joint -Massive, or thick bedded: > 1m -Bedding plane inclination > 5°	hard, cavernous, lapies, φ = 32-50	Karstification
Caliche limestone, wackestone	Dome (Sigmoid, Mogote)	-Steep slope -Slope: 30°-45° -Height: 20-50 m	-Joint -Massive or bedded -Relatively horizontal bedding plane: < 5°	hard, cavernous, lapies, φ = 32-50	Karstification Calichification
Caliche limestone, wackestone	Convex	-Gentle slope -Slope: 12°-20° -Height: 10-30 m	-Joint -With or without bedding plane -Relatively horizontal bedding plane: < 5°	weak, chalky, uncavernous φ = 17-31	Calichification
Bedded limestone, caliche limestone	Ridge	-Moderately inclined -To steep slope -Slope: 20°-35° -Top plane -Height: 10-30 m	-Joint -Thin bedded: < 1 m -Relatively horizontal: < 5°	hard, cavernous, lapies, φ = 32-50 Weak, chalky, uncavernous φ = 17-31	Karstification Calichification

Table 4   Model of the influence of lithologic physical properties and geologic structures to negative relief karst morphology.

| | Morphology | | | Morphogenesis | |
Lithology	Morphographic	Morphometric	Active morphostructure (geologic structures)	Passive morphostructure (physical properties)	Morphodynamic (exogenic processes)
Reef limestone, boundstone, bedded limestone, grainstone, packstone	Cave	-Various height, reaching 30 m -Various width, reaching 50 m	-Joint -Massive or bedded -Incline to horizontal bedding plane	Hard, cavernous, lapies, $\varphi = 32\text{-}50$	Karstification
Bedded limestone packstone, wackestone	Shaft	-Diameter of the hole: 10 m-50 m -Depth: 20 m-60 m	-Joint -Bedded -Gently incline to horizontal bedded plane : $< 5^o$	Hard, cavernous, lapies, $\varphi = 32\text{-}50$	Karstification
Reef limestone, bedded limestone, packstone, wackestone	Dolina (doline), uvala	-Steep slope -Slope: $30^o\text{-}40^o$ -Depth: 20 m-50 m	-Massive of bedded -Incline bedding plane: $> 5^o$	Hard, cavernous, lapies, $\varphi = 32\text{-}50$	Karstification
Bedded limestone, caliche limestone	Polje	-Moderately inclined to steep slope -Slope: $20^o\text{-}30^o$ -Base plane -Maximum depth: 10 m -Area: 500 m^2-1500 m^2	-Bedded -Relatively horizontal bedding plane: $< 5^o$	Hard, cavernous, lapies, $\varphi = 32\text{-}50$ Weak, chalky, uncavernous $\varphi = 17\text{-}31$	Karstification Calichification

including tectonic, and morphodynamic. It is also related to exogenic processes such as erosion, dissolution, and mass wasting.

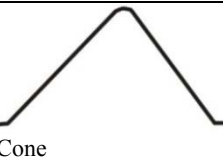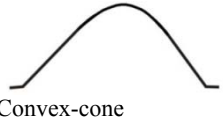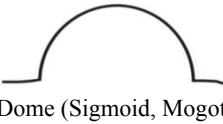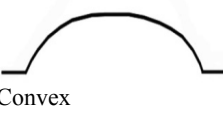Geomorphologic diversity of Gunungsewu area involves positive and negative reliefs. Positive relief comprises hills of 10 m to 90 m height. The shape varies from conical (angular top cone), dome, rounded top cone (convex-cone), convex, and ridge. While negative reliefs include doline, uvala, polje, and shaft, or cave.

Attractive morphology is not only found on the surface, but also in subsurface or in caves. There are various ornaments such as stalactite, stalagmite, pilar, sinter, and flowstones. The formation of endokarst in the caves is also influenced by the existence of fracture structures and bedding planes. The stalactites are always found in longitudinal raw following strike of fractures that is crosscutting the wall or roof of the cave.

Tables 3-4 describe the model of karst morphology of Gunungsewu area. As already discussed above, it is controlled by variation of physical properties of the lithology and the existence of geologic structures.

7. Conclusions

Results of this study and analyses on the geomorphology of Gunungsewu Area conclude that:

Karst morphology of Gunungsewu area can be grouped into morphology with positive relief including hills of cone, convex-cone, dome, convex and ridge shapes, and morphology with negative relief such as cave, shaft, doline, uvala, locva, and polje;

The variation of karst morphology of Gunungsewu area is influenced by the variation of physical properties of the lithology such as hardness and internal friction angle, and geologic structures such as joint

orientation, and existence, position, thickness of bedding plane;

Karstic limestone either massive or bedded forms hills of cone, convex-cone and dome shaped, while caliche limestone displays convex hills. Internal friction angle (φ) of the lithology determines the angle of slope inclination of the hills that are formed. The higher the value of friction angle (φ), the steeper the slope of hills which are formed;

Joint, crack and fault patterns are correlated to the lineaments of hills and valleys of the Gunungsewu area. Position and thickness of bedding plane also controls the shape of the hills: thin inclined bedding plane will result cone shape, thick inclined bedding plane will result convex-cone, while gentle to horizontal bedding plane will result dome, convex, and ridge shapes;

Cave, shaft, doline, and uvala are only formed in karstic limestone, while polje can be found either in karstic or caliche limestone.

Acknowledgment

References

[1] Kusumayudha, S. B. 2011. "Exploring the Prospective of Gunungsewu Area for a World Geopark." Presented at the Malaysia-Indonesia Join Geoheritage Convention, Terengganu, Malaysia.

[2] Van Bemmelen, R. W. 1949. *The Geology of Indonesia.* Vol IA. Hague: Martinus Nijhoff.

[3] Suyoto. 1994. "Stratigraphic Sequence of the Gunungsewu Carbonates." In *Proceedings of the PIT IAGI XXIII,* 19-32.

[4] Kusumayudha, S. B., 2004. *Introduction of Karst Hydrogeology.* Yogyakarta: Karst Study Center UPN "Veteran".

[5] Kusumayudha, S. B., Zen, M. T., Notosiswoyo, S., and Gautama, R. S. 1999. "Hydrogeologic System of Gunungsewu Area." In *Proceedings of the IAGI The 28th Annual Convention,* 73-84.

[6] Kusumayudha, S. B., Zen, M. T., Notosiswoyo, S., and Gautama, R. S. 1997. "Study on the Distribution of Carbonate Rocks Based on Fractal Characteristics of the Valley Patterns and Secondary Porosity, Case: Paliyan and Surrounding Area, Gunung Kidul, DIY." *Jurnal Teknologi Mineral* 4 (2):71-86.

[7] Setiawan, J., and Kusumayudha, S. B. 2011. "Groundwater System of Gunung Kendil and Umbul Ponjong as a Unique Geoheritage." Presented at the Malaysia-Indonesia Join Geoheritage Convention, Terengganu, Malaysia.

[8] White, W. B. 1988. *Geomorphology and Hydrology of Karst Terrains.* New York: Oxford University Press.

[9] Monroe, W. H. 1976. *The Karst Landforms of Puerto Rico.* Washington, DC: United State Government Printing Office.

[10] Franklin, J. A., and Dussault, M. B. 1989. *Rock Engineering.* McGraw, USA: McGraw Hill Publishing Company.

[11] Bogli, A. 1980. *Karst Hydrology and Physical Speleology.* Berlin, Germany: Springer Berlin Heidelberg.

[12] Dunham, R. J. 1962. "Classification of Carbonate Rocks According to Depositional Texture." In *Classification of Carbonate Rocks,* edited by W.E. Ham. AAPG Memoir.

[13] Esteban, M. 1996. *Karst System from Prospect to Reservoir.* Carbonate International Ltd.

[14] Moore, C. H. 1989. *Carbonate Diagenesis and Porosity.* Amesterdam: Elsevier.

[15] Kusumayudha, S. B. 2005. *Fractal Geometry and Hydrogeology of Gunungsewu Area.* Yogyakarta: Adicita Publisher.

[16] Kusumayudha, S. B. 2008. *Karst: Cave, Underground River and Spring.* Yogyakarta: Citra Aji Parama Publisher.

[17] Verstappen, H. Th. 1983. *Applied Geomorphology.* Elsevier Science Publishers.

[18] Goodman, R. E. 1989. *Introduction to Rock Mechanics*, 2nd ed.. Chichester: John Wiley & Sons.

[19] Hoek, E., and Bray, J. W. 1981. *Rock Slope Engineering*, Revised 3rd ed. London: The Institution of Mining and Metallurgy London.

[20] Jumikis, A. R. 1983. *Rock Mechanics*, 2nd ed. Houston, Texas: Gulf Publishing Company.

Lineament Analysis Using ASTER Satellite Images in the Southern Part of the Korean Peninsula

Weon-hack Choi[1], Sung-il Cho[1], Daiei Inoue[2], Makoto Yanagida[3], Dong-hee Park[1] and Chun-joong Chang[1]

1. Central Research Institute, Korea Hydro & Nuclear Power Co., Ltd., Daejeon 305-343, Korea

2. Department of Oversea, Tokyo Electric Power Services Co., Ltd., Tokyo 135-0062, Japan

3. Tokyo branch, Hanshin Consultant Co., Ltd., Tokyo 101-0037, Japan

Abstract: Lineaments are often related to faults and lithologic boundaries and in some cases to geomorphic relief. They can be helpfully utilized by investigating active tectonics as preliminary data. In order to assess the distribution and activity of the lineaments around the coastal area of the Korean Peninsula, we have interpreted lineaments using ASTER (Advanced Space borne Thermal Emission and Reflection Radiometer) images. The lineaments range from 2 km to 50 km long and show a dominant NNW-SSE trend. The lineament density along the eastern coast line of the Korean Peninsula is higher than the densities on the southern and western coast lines. The lineament rank is La to Le. However, La and Lb are not in sufficient abundance to have a high possibility to be active. In the Pocheon region, there are Quaternary volcanic activities, and hence there is a possibility of recent crustal movement in this area. We plan to recheck the presence and activity of ASTER lineaments by aerial photographs and field investigations in the future.

Key words: Lineament, active tectonic, ASTER image, fault.

1. Introduction

The most observable features on satellite images and aerial photographs are linear shapes known as lineaments. They appear as straight or curved lines of different lengths. They are often related to faults and lithologic boundaries and in some cases to geomorphic relief [1]. There are several definitions of these linear features. O' Leary et al. [2] defined a lineament as a mappable, simple or composite linear feature of a surface, whose parts are aligned in a rectilinear or slightly curvilinear relationship. This is the generally accepted definition. Woodruff et al. [3] defined a lineament as a feature that: 1) is perceived in an image of a solid planetary body, 2) is linear and continuous, 3) has definable end points and lateral boundaries, 4) has a relatively high length-to width ratio and hence a discernible azimuth, and 5) is shown or presumed to be correlatively related to stratigraphy or geologic structures.

Aerial photographs afford the advantage of flexibility and can provide pictures from different heights, with a variety of scales and resolutions. Satellite images, in particular, are always taken from the same height, at the same time of day, and with the same viewing angle, and have the advantage of consistency and uniformity. The objectives of this study are to interpret lineaments on the Korean Peninsula and to classify the activity order of the lineaments (Fig. 1).

In this study, the lineaments were interpreted from ASTER (Advanced Space borne Thermal Emission and Reflection Radiometer) satellite images. In the case of ASTER interpretation, the global geomorphology can be distinguished at a glance to interpret the outline of the topographical features arrangement. However, it is not possible to observe the subtle geomorphologic texture that indicates the characteristics of active structures, due to the scale of 1 : 100,000, in contrast with aerial photographs, the scale

---

Corresponding author: Sung-il Cho, Ph.D., research fields: structural geology & hydrogeology. E-mail: chosi4476@khnp.co.kr.
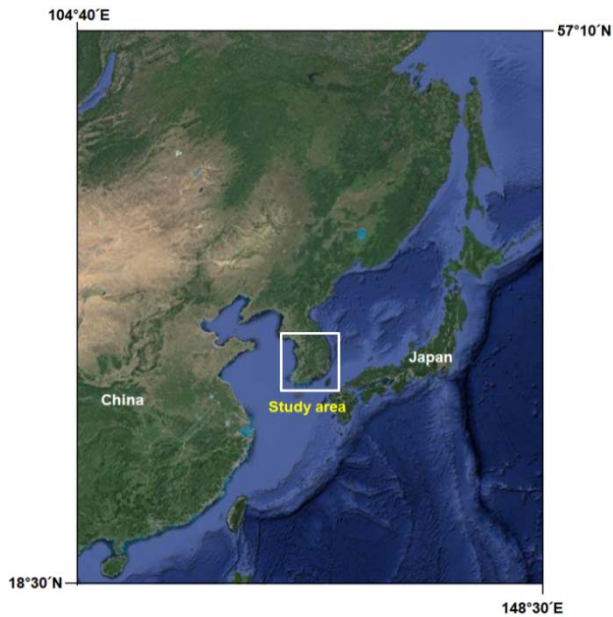
Fig. 1   Location map of the studied area.

of which is 1 : 20,000 or 1 : 50,000, of the studied area; e.g., fault scarps of 10 meter height or offset channels of 10 meters are not recognized by ASTER interpretation. Small scale deformation may be overlooked by this interpretation.

The ASTER is a sensor with 14 band wavelengths that was loaded on the Terra satellite launched by NASA (National Aeronautics and Space Administration) in 1999 [4]. It has characteristic efficiency to view stereoscopic images using the 760-860 nano meter near infrared wavelength band of vertical and backward view ((Visible and Near Infrared band 3N (nadir), 3B (27.6 degrees from nadir)). The height of the satellite is 705 km above the earth surface; resolution on this stereoscopic band is therefore 15 meters. The ASTER images were enlarged to 1 : 100,000 scale in order to interpret the tectonic geomorphology. The area of one scene image is 60 km × 60 km. To facilitate a simple and easy interpretation, one scene is divided into six sheets. The width of one sheet is A3 size of 420 mm × 297 mm.

2. Lineament Analysis

The important technical points of ASTER image interpretation are to observe the large-scale arrangement of topographical features and the height differences of mountains. Lineaments that indicate active tectonics such as active faults, active flexures, etc. are plotted regardless of whether crustal movement is conceivable to explain the above large-scale causes. For example, abrupt changes of mountain height may indicate the presence of a fault that has lifted up the mountain. Nevertheless, it is recommended that existence and activity of lineaments as determined by ASTER images be rechecked by aerial photographs and field investigations. The marine terraces of extensions of lineaments revealed by ASTER should in particular be reexamined by aerial photographs. It is very important for the evaluation to ascertain whether an individual lineament recognized by ASTER affects the deformation on terraces.

When a piedmont line is composed of a straight and steep slope, there may be an active tectonic relief such as potential active faults or buried active faults. On the contrary, it might be alternatively be interpreted as resulting from a differential erosion process by interpreting the surface texture of mountains, valley density, slope inclination, etc. of the surrounding mountains. The ASTER interpretation is superior to the aerial photograph interpretation for this judgment. In this light, ASTER image interpretation can cover a wide range at once and it is possible to compare differences.

Meanwhile, it is relatively easy to observe small fault scarps and offsets of small channels and ridges on terraces by means of aerial photograph interpretation, whereas it is often difficult by means of ASTER interpretation. But ASTER markedly excels in interpreting sharp reverse scarplets when the height differences are more than 20 meters.

The activity order on the lineaments was classified on the basis of Table 1. The lineaments judged by the ASTER study ranked from La to Ld. The La lineaments cannot be recognized in mountainous district geographical features alone. It is conclusive evidence whether there is displacement in a terrace and

Table 1   Lineament interpretation criteria for the ASTER image.

Lineament rank	Definition	Terraces, small scale stream	Large scale valley and ridge	Mountain, hill, basin
Ｌa	Certain tectonic relief	・The cliff and reverse scarplet in the same direction are recognized on the terrace surface and the talus slope in the lineament extension. ・There is a reverse inclination on the higher terrace and the back of the hill. ・The lateral offsets are in plural valley and ridge systematically develop.	This rank cannot be recognized in mountainous district geographical features alone. It is conclusive evidence of whether there is displacement in a terrace and a small-scale valley.	・This rank cannot be recognized in mountainous district geographical features alone. It is conclusive evidence of whether there is displacement in a terrace and a small-scale valley.
Ｌb	Probable tectonic relief (50%)	・The cliff and the reverse scarplet in the same direction are indistinctly recognized on the terrace surface and the talus slope in the lineament extension. ・The reverse inclination is presumed to be a higher terrace and the summit level of the hill. ・The lateral offsets are in plural valley and ridge systematically develop.	Two or more large valley and ridge offsets.	・There is discontinuity in the arrangement of large geographical features and the altitudinal distribution of the mountainous district, and tectonic movement is assumed to explain the large geomorphology. ・There are narrow basins and valleys that continue in a straight direction for considerable length, and tectonic movement is assumed to explain big geomorphology. ・The foot of a mountain line is consecutively straight line and steep inclination, and tectonic relief is assumed.
Ｌc	Probable tectonic relief (20%-30%)	・Cliff in the same direction is recognized on the terrace surface in the lineament extension, locally. ・The reverse inclination is presumed to be a higher terrace and a summit level hill.	A part of a large valley and the ridge shift systematically offsets.	・There is a high discontinuity about the arrangement of large geographical features and altitudinal distribution of the mountainous district. However, the terrain feature are insufficient as a lineament. ・There are narrow basins and valleys that continue in a straight direction for considerable length. However, the terrain feature is insufficient as a lineament. ・The foot of the mountain forms a straight line and has a steep inclination. However, the terrain features are a insufficient as a lineament.
Ｌd	Low possibility of tectonic relief (because the possibility of the an active fault cannot be denied, extract it for attention)	Scarp on the terrace surface and lateral offsets in a small-scale valley cannot be admitted.	・Offset is not admitted in a big valley and the ridge. ・There are a valley and a ridge that are not offset.	・There is highly discontinuity about arrangement of large geographical features and altitudinal distribution of the mountainous district. However, the terrain features are insufficient as a lineament. ・There are narrow basins and valleys that continue in a straight direction for considerable length. However, the terrain features are insufficient as a lineament. ・The foot of the mountain forms a straight line and has a steep inclination. However, the terrain features are insufficient as a lineament.
Ｌe	No tectonic relief (erosional geomorphology correlating with old fault, bedding stratification, and intrusive boundary)	Scarp on the terrace surface and lateral offsets in a small-scale valley cannot be admitted.	・There is no systematical offset of valleys and ridges. ・It offsets oppositely.	・There is no discontinuity about the arrangement of large geographical features and altitudinal distribution of the mountainous area, although there are straight geographical features. ・There are narrow basins and valleys that continue in a straight direction for considerable length. But the geographical features array bends, and it is regional. ・Although the foot of the mountain line forms straight line and step slope, the geographical features array bends, and regional.

a small-scale valley. Those of Lb rank have discontinuity in large geographical features arrangement and the altitudinal distribution of the mountainous district, and requires assumption of tectonic movement to explain large geomorphology. There are narrow basins and valleys that continue in straight, direction for a significant distance, and this requires assumption of tectonic movement to explain the large geomorphology. The Lc lineaments have high discontinuity for the large geographical features and altitudinal distribution of the mountainous district. However, the terrain features are a insufficient as a lineament. Those of Le rank with longer lineaments have been plotted on the sheets. The Le lineaments do not necessarily suggest active faults but may be the result of geological phenomena such as old faults, geological boundaries, etc.

The lineament rank should be regarded as commonly applicable both for ASTER lineament and aerial photograph lineament for the practical use of engineering geology. However, this ASTER interpretation study is a preliminary step; a further analysis of the relationship between ASTER and aerial photograph lineaments in terms of existence is necessary.

3. Results and Interpretation

3.1 Eastern Coast of Korean Peninsula

The investigated area is along the eastern coast of the Korean Peninsula from the border of North Korea to the city Busan. The analysis range from the coast line is roughly 20 km into inland, because the goal of this study is to investigate active faults along the coastal line.

Sixty-nine lineaments were interpreted at the eastern Korean Peninsula from 20 sheets of ASTER images (Fig. 2). Long lineaments that do not suggest active fault are also selected to illustrate old faults or geological boundaries. The lineaments dominantly have a NNE-SSW orientation and range from 2 km to 30 km long.

(a) Northern part

(b) Southern part
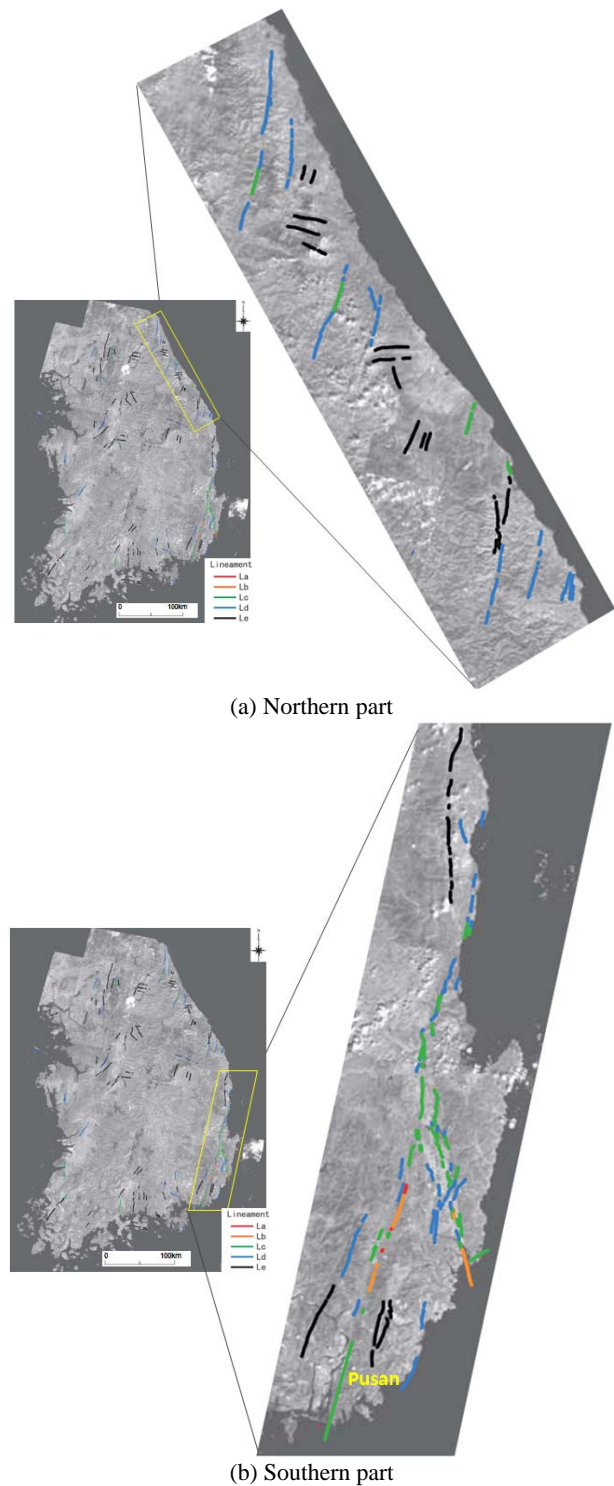
Fig. 2 Lineament map interpreted by ASTER image around the eastern coast of the Korean Peninsula.

The lineaments ascertained by the ASTER study are ranked from La to Ld. Those of Le rank with greater length have been plotted on the sheets. The Le lineaments do not necessarily suggest active faults but

may be the result of geological phenomena such as old faults, geological boundaries, etc.

The Osipcheon fault with a NNE-SSW orientation is situated along the Osipcheon River (Fig. 3). The Osipcheon lineament is divided into three segments. However, the geological faults that may cause the lineament continue without gap as the Osipcheon fault system. The Osipcheon lineament may partly coincide with a geological fault, but the whole line has almost no relationship with the fault shown in the geological map. The Yangsan faults and the Ulsan faults are well known active faults (Fig 3). The Yangsan lineaments are covered by alluvial sediment, and consequently there is no information on activity. There are several dextral offsets of small gorge and ridges. Numerous studies on trench results and active fault outcrops along this lineament have been carried out [5-7].

The Ulsan lineaments globally have a relationship with the Ulsan fault system that forms the uplift of the eastern mountains. The partial lineaments are interpreted as faults that caused subsidence of the eastern basin. The lineament positions between aerial photographs and ASTER interpretation sometimes differ, because it is difficult to interpret small scale precise geomorphologic features by ASTER. The exact position should be decided by aerial photograph interpretation. ASTER images support that there is an active tectonic topography between mountains and plains.

3.2 Southern Coast of Korean Peninsula

The interpretation of ASTER images was carried out from Busan city to Jindo Island via Masan and Gwangyang along the south coast line. The interpretation region to the inland direction is generally about 30 km from the coast line, but the width differs scene by scene. Twenty-three lineaments were interpreted at the southern part of the Korean Peninsula from 11 ASTER scenes (Fig. 4).

The dominant orientation of the lineaments is NNE-SSW and NE-SW. The lineaments range from 6

Fig. 3 Comparison of lineaments by ASTER image to geological structures around the eastern Korean Peninsula. (A) Lineaments map by ASTER image, (B) Geological map [8].
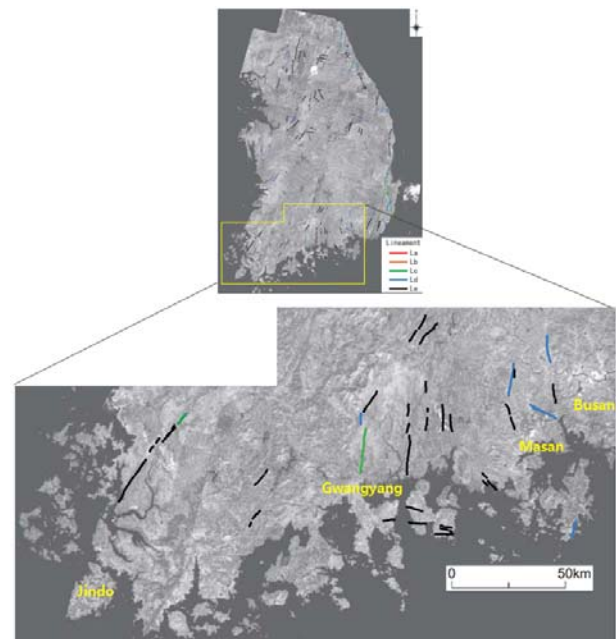
Fig. 4 Lineament map interpreted by an ASTER image around the southern coast of the Korean Peninsula.

km to 50 km long and rank from Lc to Le activity. There are hills of peneplain blocks on the lower land with elevation less than 200 meters in the southern Korean Peninsula. These hills are composed of close valley spacing.

3.3 Western Coast of Korean Peninsula

The interpretation region is from Buan to Imjin River along the border with North Korea. Seven lineaments were interpreted. The lineaments have a dominant NNE-SSW orientation and range from 6 km to 26 km long (Fig. 5). The lineament rank is Ld and Le, except for the Buan lineament of Lc rank. The Ld and Le rank lineaments have little possibility of being active.

3.4 Southern Korean Peninsula

The ASTER interpretation region is about 100 km

from north to south and about 60 km from east to west of Pocheon, Gyeonggi province (Fig. 6).

The lineaments are classified as Lc, Ld and Le. The study area is located north of Seoul. The mountain ranges are distributed in N-S and NNE-SSW directions. According to the geological map with a scale of 1 : 250,000, the Quaternary basalts are colored in this region [9].

Ten lineaments at the Pocheon region are interpreted (Fig. 6). Uplands and hills that were formed by Quaternary volcanic products along the river and in the basin were recognized. These volcanic products are distributed in a 20 km wide range, and uplands are formed by these rocks. There are volcanic products of several ages, and some of them formed hill topography. Distinct craters or calderas do not remain, but the basin is estimated to be the center of eruption, due to the distribution of huge volcanic products. Looking at the far northern part by means of Google Earth, there are three caldera-like topographies. According to the above geological map, these volcanic products are basalt, but there is another possibility that they are large scale pyro-clastic flow or thin wide flood basalt. In any case, these basaltic rocks were produced during the Quaternary age by monogenetic volcanoes.

There are many lineaments with N-S and NNE-SSW

Fig. 5   Lineament map interpreted by ASTER image around the western part of the Korean Peninsula.
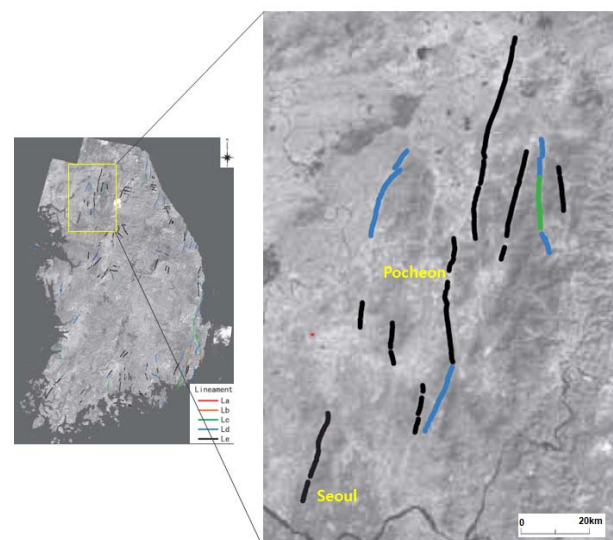
Fig. 6   Lineament map interpreted by ASTER image around the southern part of the Korean Peninsula.

orientations in the studied area. There are also Quaternary volcanic activities in this area, and hence there may be the possibility of recent crustal movement in this area. The lineament density of this area is higher than that of the coastal area of the Korean Peninsula, and the same density as that of the Yangsan and Ulsan fault areas. However, the lineament rank is lower than that of the Yangsan and Ulsan fault areas.

3.4 General Interpretation

3.4.1 Predominant Orientation of the Lineaments

Major geological structures of Precambrian gneiss, crystalline schist, granite etc. in Korean Peninsula are oriented in the NNE-SSW direction. The large scale faults that separate large geological structures and divide the Korean Peninsula along the NNE-SSW direction can be easily delineated by using small scale satellite images such as Landsat images. These faults are 200-400 km long. The dominant orientation of lineaments in this study area is also NNE-SSW, consistent with the geological structure (Fig. 3). Kim and Seo [10] released a lineament map of the Korean Peninsula based on a Landsat satellite image (Fig. 7). They reported that the dominant orientation of the lineament is from NNE to NE.

The recent activity may be the inversion movement of old faults. The lineament density along the eastern coast of the Korean Peninsula is higher than that along the southern and western coasts.

3.4.2 Length of the Lineaments

Active or probable active parts of faults with a NNE-SSW orientation such as the Osipcheon fault (Fig. 3), and several lineaments interpreted by means of ASTER image do not continue for long distances, being from 10 to 40 km long, compared with the original fault length. The faults that divide the geological distribution continue for several hundred kilometers, based on interpretation of topographic maps. Using ASTER images that correspond to 1 : 100,000 scale topographic maps, it is found that lineaments are interrupted by ridges or hills, and do not

continue over long distances.

3.4.3 Lineaments Activity

The Yangsan faults and the Ulsan faults are well known active faults (Fig. 4). The Yangsan fault is a right lateral fault and has a NNE-SSW orientation. A lineament that is located near the eastern coast is right lateral with a NNE-SSW orientation. This is ranked as Lc rank. While evidence that the above faults are active has not been confirmed, there is a possibility that they are active, because they have clear topography as active faults. On the other hand, there are only three Ld rank lineaments, and all the others are Le rank lineaments in this study. They are judged to be Le rank because there are no height differences across the lineaments or the lineaments have smooth curves that are free from roughness as a result of being controlled by the schistosity or bedding plane.

3.4.4 Uneven Distribution of Lineaments

This is an assumption in terms of the geomorphologic situation that lineaments that are located along the eastern coast line do not continue
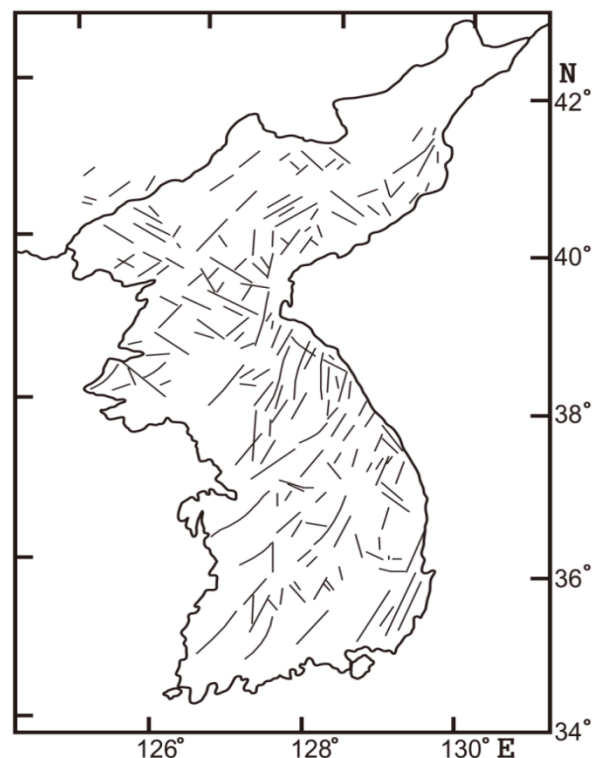
Fig. 7   A lineament map from a Landsat satellite image of Korean Peninsula [10].

inland. The faults are more than 100 km long from a geological point of view, but the lineaments do not continue for long distances and they are distributed fragmentally. Active lineaments, including fragmental lineaments that are unevenly distributed, are limited to the east coast of the Korean Peninsula.

3.4.5 Long Faults that Form Geological Structure

Why were the topographic features that correspond to long faults formed? One answer is that intermitted lineaments were formed by the erosion process. On the other hand, the lineaments interpreted by the ASTER image are less than 40 km long. There are seven NNE-SSW lineaments in this study. One is Lc and Ld, five are Ld, and one is Le. These NNE-SSW orientation lineaments might be active; otherwise, they are remnants that were moved during the Neogene.

3.4.6 E-W Lineaments

There are seven E-W orientation lineaments. These lineaments appear to be systematically distributed and have the same separation between them. But the lineaments range from 5 to 34 km long. It is difficult to estimate the cause of the lineament formation. They may be formed by joints, but if so, the joints were very long. These lineaments might have been formed the differential erosion of different basement rock types.

5. Future Study

The lineament rank should be regarded as commonly applicable for ASTER lineaments for the practical use of engineering geology. However, the present ASTER images interpretation study is a preliminary step; analysis of the relationship between ASTER and aerial photograph lineaments with respect to their existence and rank has not yet been carried out. We plan to recheck the existence and activity of ASTER lineaments by aerial photographs and field investigations.

Marine terraces of extended of lineaments revealed by ASTER should in particular be reexamined by aerial photographs. It is very important for the evaluation to determine whether an individual

lineament recognized by ASTER affects the deformation on the terrace. Hence, we interpreted the above area by means of ASTER images, considering that we have information on the fault outcrops, the existence of lineaments, and terrace deformation. The ASTER sheet is very convenient to view the broad geomorphologic active tectonics in terms of the cause of geomorphology. We will use both precise lineament maps by large scale aerial photographs and broad active tectonic maps by small scale ASTER images.

6. Conclusions

In this study, the lineaments around the coastal area of the Korean Peninsula were interpreted by ASTER images. The lineaments range from 2 km to 50 km long and show a dominant NNW-SSE trend, consistent with the geological structure. The lineaments assessed by the ASTER study ranked from La to Le. However, La and Lb are not in sufficient abundance that they would have a high possibility of being active. The lineament density along the Eastern coast of the Korean Peninsula is higher than that along the southern and western coast, respectively. In the Pocheon region, there are Quaternary volcanic activities, and hence there is a possibility of recent crustal movement in this area. We plan to recheck the existence and activity of ASTER lineaments by aerial photographs and field investigations in the future.

Acknowledgments

References

[1]   Hariri, M. 1995. "Lineaments Studies and Fracture Control on the Tertiary Gold-Silver Deposits, Northern Black Hills, South Dakota, USA." Ph.D. thesis, South Dakota School of Mines and Technology.

[2] O' Leary, D., Friedman, D., and Poh, H. 1976. "Lineaments, Linear, Lineations: Some Standards for Old Terms." *Geological Society of America Bulletin* 87 (10): 1463-69.

[3] Woodruff, K., Talley, J., and Miller, J. 1982. *Selection of Sites for High Productivity Well. Maryland America. Abstracts with Programs.* Baltimore: N.E. Geol Soc Am.

[4] Abrams, M., and Ramachadram, S. 2003. *ASTER User Handbook*. Pasadena: Jet Propulsion laboratory.

[5] Kyung, J. B. 2003. "Paleoseismology of the Yangsan Fault southeastern part of the Korean Peninsula." *Annals of Geophysics* 46 (5): 983-96.

[6] Park, Y. D., Ree, J. H., and Yoo, S. H. 2006. "Fault Slip Analysis of Quaternary Faults in Southeastern Korea." *Gondwana Research* 9 (1-2): 118-25.

[7] KIGAM (Korea Institute of Geoscience and Mineral Resources). 1995. *Geological Map in Korea (1 : 1,000,000)*. Daejeon: KIGAM.

[8] Inoue, D., and Choi, W. H. 2006. *The Activity of the Ulsan Fault System Based on Marine Terrace Age Study at the Southeastern Part of Korean Peninsula*. CRIEPI report: N 05012.

[9] KIGAM (Korea Institute of Geoscience and Mineral Resources). 1999. *Explanatory Note of the Seoul-Namchonjeom Sheet (1 : 250,000)*. Daejeon: KIGAM.

[10] Kim, K. D., and Seo, J. H. 1977. "A Study on the Characteristics and the Causes of Earthquakes in Korea." *Jour. Korean Institute of Mineral and Mining Engineers* 14 (4): 240-68.

The Influence of Soil Characteristics in Seismic Response of Embedded Structures

Adrian Popovici, Cornel Ilinca and Răzvan Vârvorea

Department of Hydrotechnics Engineering, Technical University of Civil Engineering, Bucharest 020396, Romania

Abstract: The seismic response of a large wastewater collector box-type is performed by spectral analysis and direct time integration methods. The influence of mechanical characteristics of surrounding soil on structure seismic response is investigated. For this purpose the soil bulk modulus was successively considered 40,000 kPa and 80,000 kPa. The study points out the kinematic interaction soil-buried structure is usually more important than inertial interaction. Over wastewater collector is placed a river channel with 2.30 m deep water. The analysis shown the water from river channel led to significant increase in structure sectional stresses during seismic action.

Key words: Embedded structures, seismic response, parametric study.

1. Introduction

Dambovitza river crosses Bucharest city, the capital of Romania from north-west to south-east. The river is the main collector of rainwater and groundwater from city area. Over the centuries in the river was also discharged wastewater from the city sewerage system. Therefore while the river became increasingly polluted and no longer met environmental requirements [1].

Between 1984-1988 on Dambovitza river in Bucharest area along of 10 km were carried out extensive rehabilitation works. The river bed was deepened in order to carry out the main collector channel as reinforced concrete structure of compartmented box—type for the city's wastewater. Above of box-type structure, separated by a common floor, the river was channeled and fragmented in a cascade consisting of seven small reservoirs created by river dams. In order to control the flow along cascade on Dambovitza river, upstream of Bucharest city was carried out an important artificial reservoir named Lacul Morii with volume of 20 million m^3 for flood control and multy-years regulation of the river flow. In

Fig. 1 is presented a typical cross section of the Dambovitza development in Bucharest, Ciurel—Opera sector, about 2 km downstream of Lacul Morii reservoir.

Bucharest city is located in an area of highest seismicity generated by well known Vrancea hypocenter. The statistics shown that Vrancea hypocenter generates two-three destructive strong subcrustal earthquakes per century. The last Vrancea destructive earthquake with 7.4 magnitude was at 4th March 1977 provoking 1,530 human victims and 11,300 wounded from which 90% were in Bucharest and very important material losses (about 2 billion US$). Fig. 2 illustrates two accelerograms of Bucharest—Vrancea 4th March 1977 earthquake recorded in subsoil of a building from the city [2].

In the conditions mentioned before, the seismic safety of the main collector for wastewater needed a special attention in design and operation. The seismic safety of buried (embedded) structures is essentially influenced by the dynamic behavior of the surrounding deposit. In the present case, taking into account, the collector conveys continuously the wastewater and over it exists the artificial channel bed of Dambovitza river, the seismic interaction water—structure is also important for seismic response of the structure [3-7].

Corresponding author: Adrian Popovici, professor, research fields: hydraulic construction and earthquake engineering. E-mail: popovici@utcb.ro.
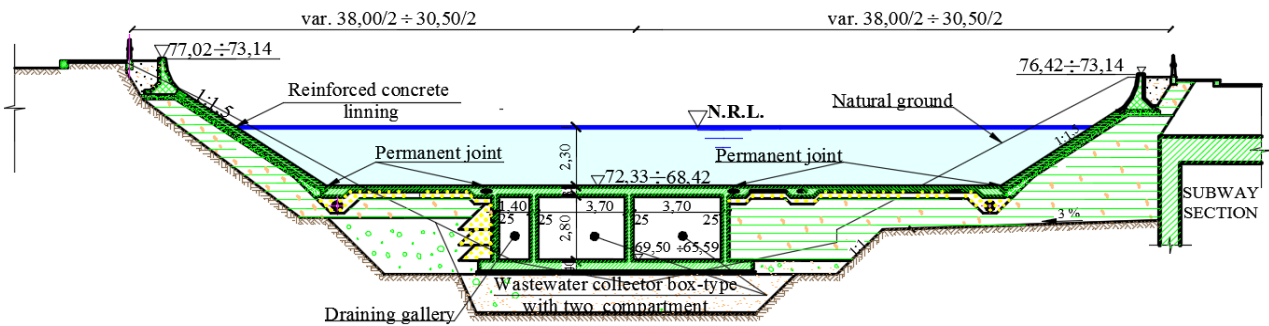
Fig. 1   Cross section through Dambovitza river development in Bucharest city, Opera—Ciurel sector.
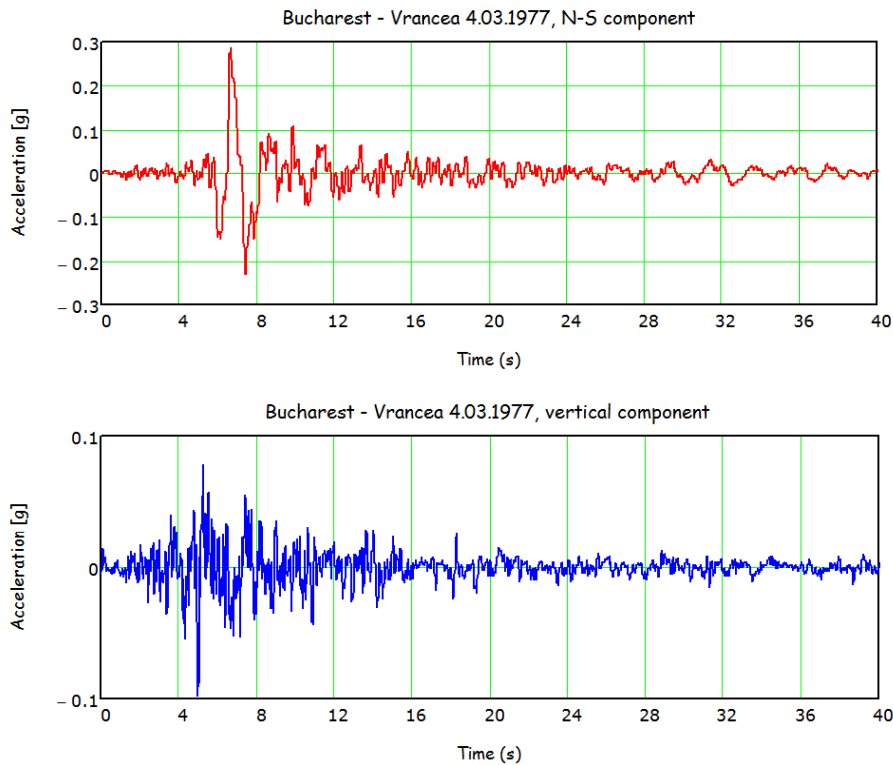
Fig. 2   Accelerograms Bucharest–Vrancea 4.03.1977 earthquake recorded in a building subsoil from Bucharest city: N-S component and vertical component.

The potential errors introduced by ignoring the interaction effects of structure with surrounding soil and water can certainly not be overlooked.

As the structure is relatively stiff compared with adjacent soil, the ground motions are constrained. This phenomenon called "kinematic interaction" depends on the geometrical and stiffness configuration of the structure, soil characteristics and variation of the seismic waves. Usually the kinematic interaction effect on the seismic response is dominant in comparison with the influence of inertial soil—structure interaction.

The parameters of interest in soil—structure interaction analysis are strains and stresses, not acceleration of the soil.

Direct solutions of complete soil-fluid-structure interaction approach can be obtained by FEM (finite element method). This technique is applied in the present paper.

The laboratory and in site tests results concerning soil characteristics have shown big scattering. In order to evaluate the influence of the soil characteristics on seismic response of the embedded structure, the

analyses were performed for two hypotheses concerning soil characteristics: pessimistic and respectively, optimistic one. They were the envelopes of test results.

The hydrodynamic effects of water contained in collector and from river channel, generated by earthquake were considered using added mass procedure based on Westergaard relation and acoustic finite elements based on Helmholtz bi-dimensional differential equation.

The accelerograms from Fig. 2 of the Bucharest-Vrancea 04.03.1977 earthquake were applied at the boundaries of the finite element mesh, successively on horizontal direction and horizontal + vertical directions.

The seismic analyses were performed taking into account the linear elastic behavior of materials using Abaqus software. The structure response was computed by spectral analysis method and direct time integration method, the results being compared and commented [8].

The sectional stresses acting on collector structure in spectral analysis were evaluated in compliance with RSS (Root Sum Square) relation of the stresses in representative mode shapes.

Finally is pointed out the seismic vulnerability of the structure analyzed including the influence of the surrounding soil. Generally, the results can be extended to other embedded (buried) structures.

2. Mathematical Model and Input Data

Fig. 3 illustrates finite element mesh of the foundation-water-structure unitary system in compliance with Abaqus software. The extension of the foundation was chosen in order to avoid the influence of boundary conditions on seismic response of the structure.

The structure (collector) was modeled with beam elements (B22-A3 node quadratic beam in a plane). The foundation was discretized with quadrilateral plane strain elements (CPS4: A4 node bilinear plane stress quadrilateral). The water from collector and Dambovitza channel was discretized with quadratic elements 2-D acoustic (AC2D8: A8 node quadratic 2-D acoustic quadrilateral). The analysis was performed for 1 m along Dambovitza river development.
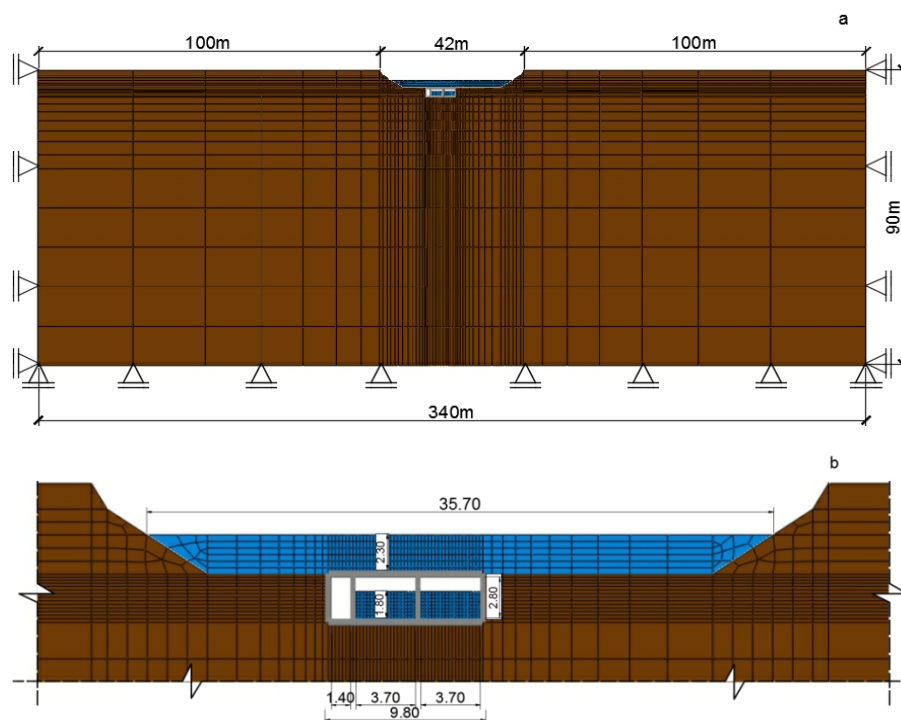
Fig. 3   Finite element mesh of the foundation-water-structure unitary system: a-general, b-detail.

The boundary conditions were applied at the limits of the mesh, as follows: at the bottom, translations on y direction (vertically) were blocked, excepting corner nodes were the both translations on x and y directions were blocked and at the both lateral limits, the translations on x direction (horizontally) were blocked.

In Table 1 is shown some data about finite element mesh, respectively the number of the nodes and elements for each subsystem.

The properties of materials from the system are presented in Table 2. It may be remarked that for foundation soil two characteristics, pessimistic and optimistic were successively considered.

In order to perform spectral analysis, design spectra were necessary to be evaluated from the accelerograms presented in the Fig. 2. They were computed using well-known relation with convolution integral. Design spectra were obtained by smoothing the values from response spectra according to the rules of the least squares. Design spectra for both accelerograms and fraction of the critical damping $v = 0.05$ are presented in Fig. 4.

Damping matrix $[C]$ used in direct time integration method was evaluated according to linear Rayleigh relation, the coefficients α and β being computed based on two mode shapes of the system having the longest natural periods:

$$[C] = \alpha [M] + \beta [K]$$
$$\alpha = 2\, v\, \omega_1\, \omega_2/(\omega_1 + \omega_2) \text{ and } \beta = 2\, v/(\omega_1 + \omega_2)$$

where, $[M]$ and $[K]$ are mass matrix and stiffness matrix;

$v = 0.05$ fraction of critical damping;

$\omega_1\, \omega_2$ two shortest circular frequencies of the system (rad/s);

The α and β values calculated in different hypotheses are presented in Table 3.

For both pessimistic 40 MPa and optimistic 80 MPa characteristics of the foundation soil, the load combinations considered in seismic response of the Bucharest main collector for wastewater are presented in Table 4.

3. Some Results Concerning Seismic Analysis of the Embedded Structure

The values of first six longest natural periods of the foundation-water-structure unitary system in different hypotheses are illustrated in Fig. 5. It may be remarked the significant influence of the soil characteristics on the natural periods of the system. For instance the fundamental period increased with about 40% for a decrease of the soil bulk modulus from 80 MPa to 40 MPa.

Table 1   Data on finite element mesh.

Nodes/Elements Sub-systems	Nodes	Elements
Collector	290	146
Foundation	1,944	1,810
Water in collector	1,332	399
Water in river channel	1,140	342
Total	4,706	2,697

Table 2   Material characteristics.

Properties	Reinforced concrete	Foundation soil	Water
Mass density (kg/m^3)	2,400	0	1,000
Static Poisson coefficient	0.18	0.30	
Dynamic Poisson coefficient	0.23	0.30	
Static Young modulus (MPa)	23,000	40/80	
Dynamic Young modulus (MPa)	27,600	40/80	
Bulk modulus (MPa)			2,200

Fig. 4   Design spectra (blue color) and seismic response spectra (red color) for 5% damping rate on horizontal (a) and vertical (b) directions.

Table 3   The α and β parameters in Rayleigh relation.

Young modulus of the foundation soil (kPa)	Added mass		Acoustic elements	
	α	β	α	β
40,000	0.78322	0.00319	0.99882	0.00239
80,000	1.10372	0.00226	1,40965	0.00169

Table 4   The load combinations taken into account in seismic analyses.

Hypothesis number	E_f = 40,000 kPa/E_f = 80,000 kPa						
	Static analysis			Dynamic analysis			
				Acoustic elements		Horizontal earthquake	Vertical earthquake
	Dead weight	Hydr. prs. in collector	Hydr. prs. in channel	Water in collector	Water in channel		
1	Yes	Yes	-	Yes	-	Yes	-
2	Yes	Yes	Yes	Yes	Yes	Yes	-
3	Yes	Yes	-	Yes	-	Yes	Yes
4	Yes	Yes	Yes	Yes	Yes	Yes	Yes

Period (s) E=40MPa	1	2	3	4	5	6
Without water	0.205	0.202	0.086	0.047	0.043	0.022
Water in collector - Westergaard	0.274	0.272	0.111	0.059	0.058	0.030
Water in collector and channel- Westergaard	0.404	0.398	0.208	0.163	0.129	0.106
Water in collector - Acoustic	0.253	0.230	0.097	0.052	0.048	0.026
Water in collector and channel - Acoustic	0.382	0.247	0.180	0.149	0.117	0.100

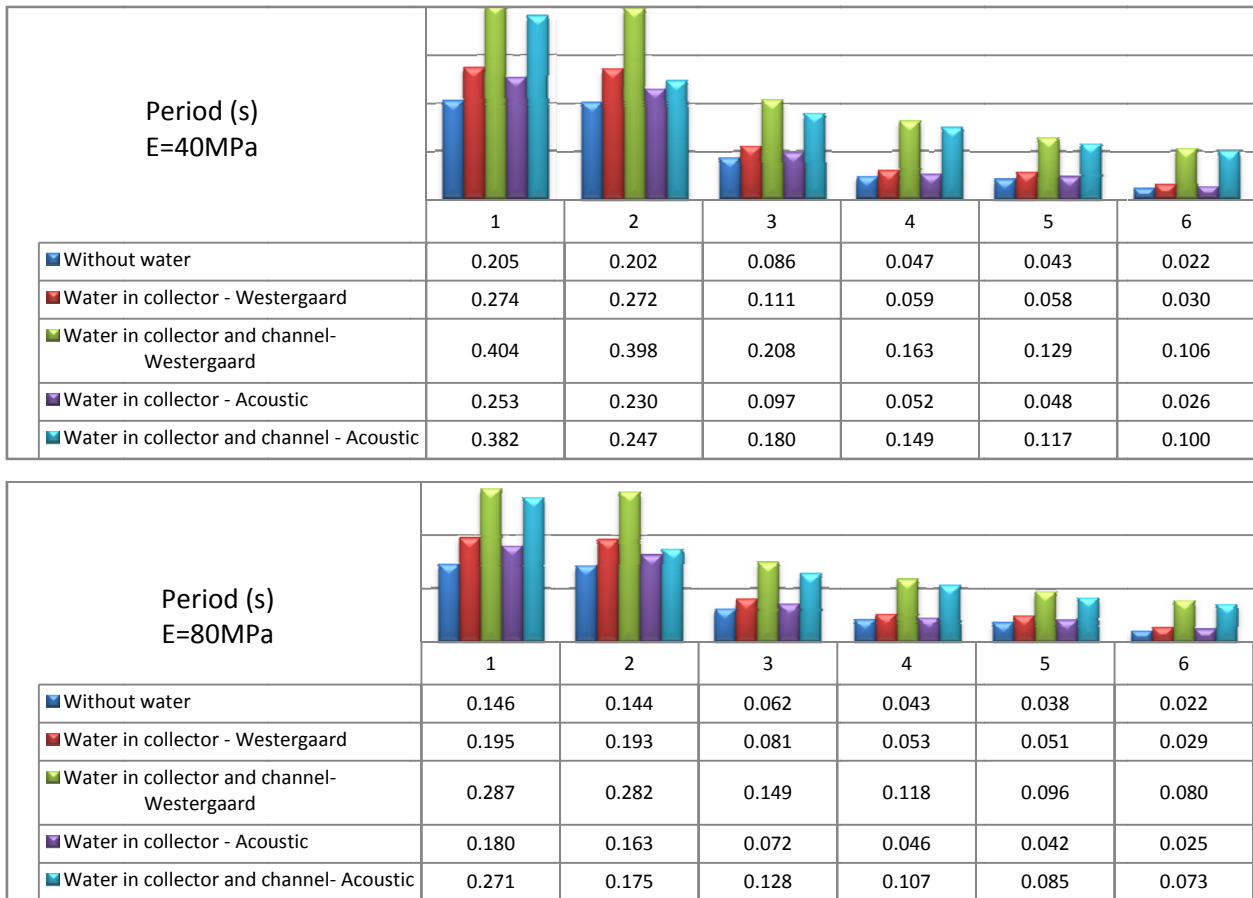| Period (s) E=80MPa	1	2	3	4	5	6
Without water	0.146	0.144	0.062	0.043	0.038	0.022
Water in collector - Westergaard	0.195	0.193	0.081	0.053	0.051	0.029
Water in collector and channel- Westergaard	0.287	0.282	0.149	0.118	0.096	0.080
Water in collector - Acoustic	0.180	0.163	0.072	0.046	0.042	0.025
Water in collector and channel- Acoustic	0.271	0.175	0.128	0.107	0.085	0.073

Fig. 5   The largest natural periods (s) of the system evaluated in different hypotheses.

The influence of the interaction with water may be also remarked. The fundamental period increased with about 90% when water exists both in collector and river channel compared to the case when they are empty. The periods evaluated by added mass approach versus equivalents evaluated with acoustic elements are longer suggesting the forces acting on structure in first case are comparatively higher. This means the added mass approach is conservative one.

Taking into account the results from free vibration analysis, the seismic response of the collector was evaluated by spectral analysis and by direct time integration method using added mass approach for interaction with water.

Father, the following notations are used for different loads acting on collector structure: G—dead load, PHC—hydrostatic pressure in collector, PHR—hydrostatic pressure in river channel, G + PFC = S, G + PHC + PHR = TS, DSH—design spectrum (Fig. 4a) of the horizontal accelerogram applied on horizontal direction, DSV—design spectrum (Fig. 4b) of the vertical accelerogram applied on vertical direction, EH—North-South accelerogram ($a_{max} = 0.19$ g) (Fig. 2a) applied on horizontal direction, EV—vertical accelerogram ($a_{max} = 0.13$ g) (Fig. 2b) applied on vertical direction.

Fig. 6 and 7 represent diagrams of bending moments (M) and axial forces (N) acting on collector structure due to load combination G + PHC + PHR ± DSH ± DSV. The structure response was evaluated by spectral analysis for $E_f = 40{,}000$ kPa and respectively, $E_f = 80{,}000$ kPa. A more comprehensive analysis of the sectional stresses (M, N) values in representative points of the collector structure in different load combinations can be made based on the data in Table 5.

In Fig. 8 are illustrated in few representative points

Fig. 6   Diagrams of bending moments (kNm/1 ml) and axial forces (kN/1 ml) of the load combination G + PHC + PHR ± DSH ± DSV resulted in spectral analysis for E_f = 40,000 kPa.
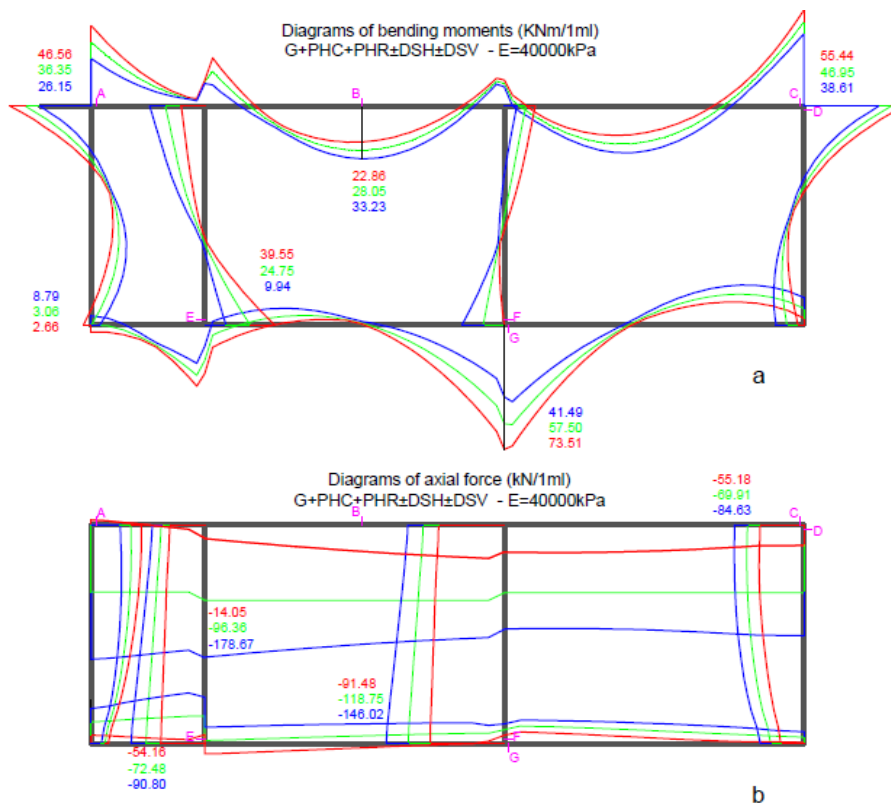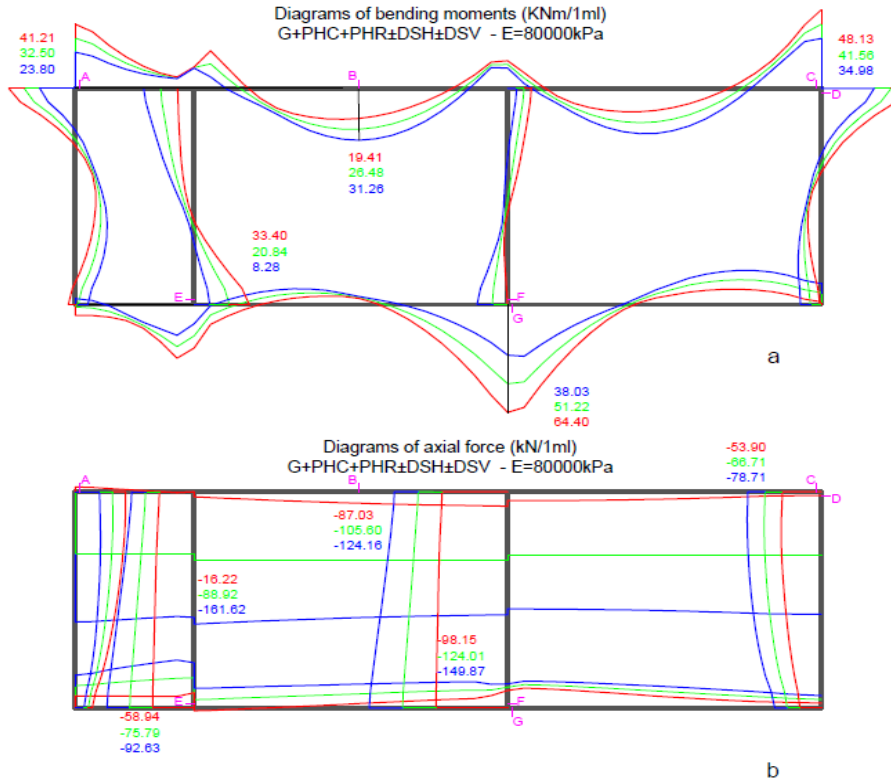

Fig. 7   Diagrams of bending moments (kNm/1 ml) and axial forces (kN/1 ml) of the load combination G + PHC + PHR ± DSH ± DSV resulted in spectral analysis for E_f = 80,000 kPa.

Table 5   **Maximum values for M and N in different hypotheses.**

Point (see Fig. 6a)	E_f = 40,000 kPa		E_f = 80,000 kPa	
	G + PHC + PHR ± DSH			
	Max. M (kNm/ml)	Max. N (kN/ml)	Max. M (kNm/ml)	Max. N (kN/ml)
A	32.55	-85.84	27.23	-77.90
B	14.55	-82.44	12.85	-71.10
C	40.28	-102.96	32.18	-88.99
D	40.28	-32.97	32.18	-28.11
E	32.03	-19.03	25.03	-21.06
F	21.88	-34.44	15.36	-39.18
G	37.21	14.70	29.94	8.18
Point (see Fig. 6a)	E_f = 40,000 kPa		E_f = 80,000 kPa	
	G + PHC + PHR ± DSH ± DSV			
	Max. M (kNm/ml)	Max. N (kN/ml)	Max. M (kNm/ml)	Max. N (kN/ml)
A	46.56	-183.16	41.21	-169.10
B	33.23	-160.00	31.26	-143.85
C	55.44	-149.92	48.13	-137.24
D	55.44	-84.63	48.13	-78.71
E	39.55	-90.80	33.40	-92.63
F	25.30	-146.02	20.47	-149.87
G	73.51	-25.28	64.40	-31.46

Note: M are represented on the tension side of the face; N (+) is tension.

(see Fig. 6a) the oscillograms of the bending moments and axial forces computed by direct time integration method during Bucharest-Vrancea NS and V 4.03.1977 earthquake and compared with the equivalent results in spectral analysis.

In compliance with Romania regulation based on Eurocode2 for calculus of the reinforced concrete section (ASRO 2004b, SREN 1992-1-1: 2004 Eurocode2) were evaluated the resistant capacity (resilience) of the collector structure components (floor, walls, apron). The results are the followings:

Floor: $M_{capable}$ = 103.3 kNm/1 ml

Apron: $M_{capable}$ = 151.9 kNm/1 ml

Wall: $N_{capable}$ = 156.0 kN/1 ml

Wall: $M_{capable}$ = 54.0 kNm/1 ml

In the hypothesis E_f = 40,000 kPa, the collector structure has comparatively higher displacements and strains than for hypothesis E_f = 80,000 kPa. In other words, a more important quota of the earthquake energy is taken out by a terrain with superior mechanical characteristics and so the embedded structure is better protected. In the case of the structure

analyzed in present paper the reduction of the bending moments for E_f = 80,000 kPa versus E_f = 40,000 kPa is in the range 13%-27%.

Another aspect needing be pointed out is concerning the effect on seismic response of the water having 2,30 m depth from river channel placed over collector. Its effect appears to be very important. Under action of DSH + DSV, the bending moments in collector structure increase in the range 32%-120% when there is water in river channel versus the case when the river channel is empty. If over embedded structure was soil instead of water, the effect should be possible diminished because of arches discharge that may arise in the field above the structure.

The comparison between corresponding results which were obtained in spectral analysis and direct time integration method (Fig. 8) emphasizes that spectral analysis led generally to higher values, so it is conservative. This conclusion is confirmed by other numerous applications [4, 5].

Concerning the capacity of the collector structure to withstand to Bucharest Vrancea 4.03.1977 earthquake,
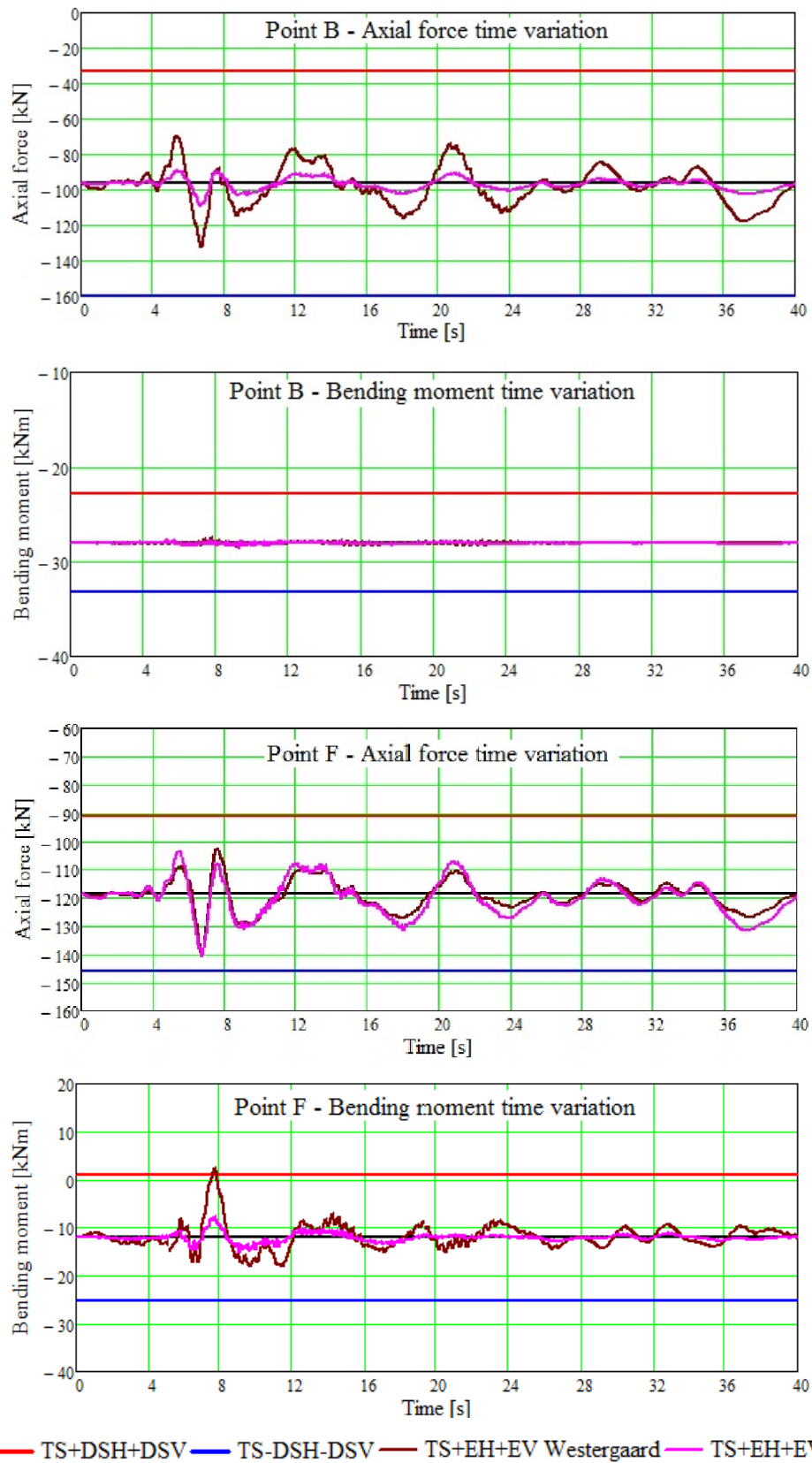
Fig. 8   Bucharest wastewater main collector—Axial forces and bending moments time variation in B and F points (see Fig. 6a) to action of the Bucharest–Vrancea 4.03.1977 N-S and V earthquake.
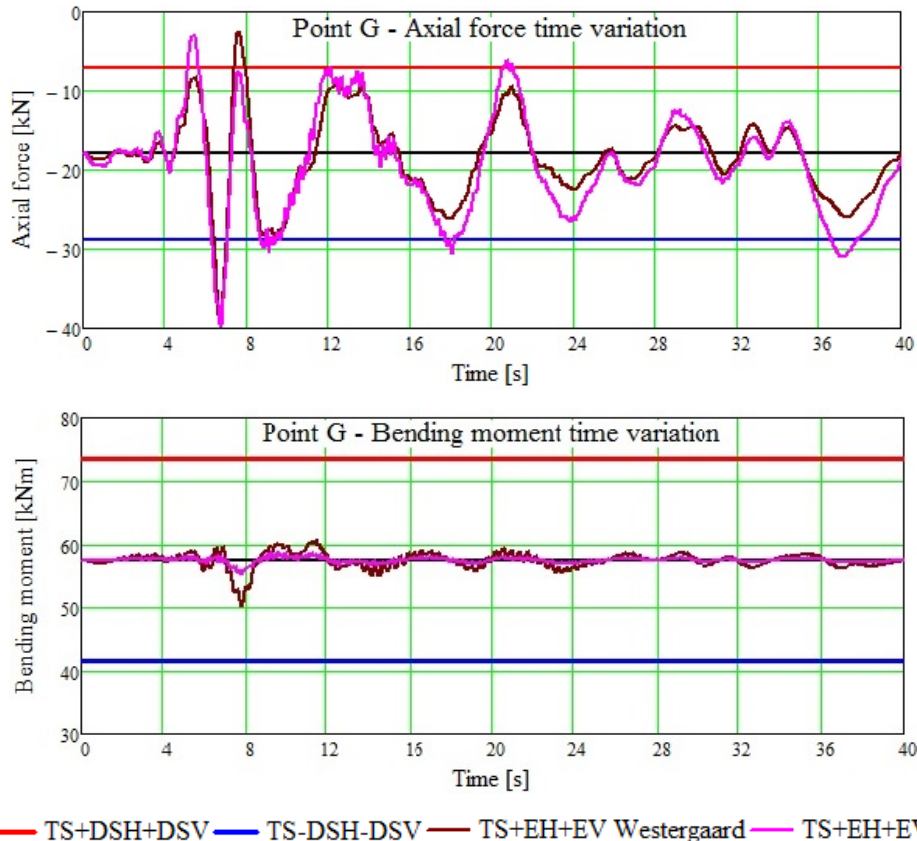
Fig. 9 Bucharest wastewater main collector—Axial forces and bending moments time variation in G point (see Fig. 6a) to action of the Bucharest–Vrancea 4.03.1977 N-S and V earthquake.

the conclusion is an optimistic one comparing the effective maximum sectional stresses on structure with structure resilience (capacity of resistance). The critical point of the structure seems to be central node wall-apron where maximum axial force developed during earthquake reaches the resilience of the wall. A potential collapse mechanism can consist of central wall collapse causing destruction of the floor.

4. Concluding Remarks

The mechanical characteristics of the soil surrounding an embedded structure have important effects on seismic response of the structure. In seismic response of embedded (buried) structures the kinematic interaction is frequently more important than inertial soil—structure interaction. In the analysis presented in this paper the fundamental period of a large wastewater collector increased with about 40% and bending moments in its structural elements increased in the range 13%-27% when surrounding soil bulk modulus varied from 80,000 kPa to 40,000 kPa.

In the analysis cited before needs remark also the very important influence on seismic response of the water having 2.30 m depth from a river channel located over wastewater collector. The bending moments in collector structure increased in the range 32%-120% when there was water in river channel versus the case when the channel was empty. This effect remains important also if over buried structure exists soil although the effect can be slightly reduced by arches discharge.

The present study was performed in the hypothesis of linear elastic behavior of materials from soil-structure system. This is a conservative hypothesis. More sophisticated constitutive relations (nonlinear, elasto–plastic etc.) concerning material behavior could reveal additional reserve of the structure resistance but they were not applied in present paper because of lack

of adequately field measurements.

References

[1] GA (Government Agency). 1988. *Dambovitza—blue Main Channel of the Romania Capital (in Romanian).* Bucharest: Editura Meridiane.

[2] Bălan, S., Cristescu, V., and Cornea, I. 1982. *Romania Earthquake March 4, 1977 (in Romanian).* Bucharest: Editura Academiei R.S.R.

[3] Popovici, A., Baubec, S., and Ghiocel, D. 1987. "Seismic Soil—Structure Interaction for Large Underground Structures." *Scientific Bulletin of Civil Engineering Institute of Bucharest* 30 (1): 29-38.

[4] Ilinca, C., Vârvorea, R., and Popovici, A. 2014. "Influence of Dynamic Analysis Methods on Seismic Response of a Buttress Dam." *Mathematical Modeling in Civil Engineering* 10 (3): 12-6.

[5] Popovici, A., Ilinca, C., and Varvorea, R. 2013. "Study on Arch Dam—Reservoir Seismic Interaction." In *Proceedings of the 12th International Benchmark Workshop on Numerical Analysis of Dams*, 123-37.

[6] Hashash, Y., Hook, J., Schmidt, B., and Chiang, Y. J. 2001. "Seismic Design and Analysis of Underground Structures." *Tunneling and Underground Space Technology* 16 (December): 247-93.

[7] Imamura, A., Ishizaki, M., Watanabe, T., and Motosaka, M. 1992. "Seismic response characteristics of embedded structures considering cross interaction." In *Proceedings of the Earthquake Engineering Tenth World Conference,* 1719-24.

[8] Abaqus Inc. 2009. *Abaqus 6.11/CAE Users Manual.* United States of America: Abaqus Inc.

Punch Multi-slice Longwall Mining System for Thick Coal Seam under Weak Geological Conditions

Takashi Sasaoka[1], Akihiro Hamanaka[1], Hideki Shimada[1], Kikuo Matsui[1], Nay Zar Lin[2] and Budi Sulistianto[3]

1. Department of Earth Resources Engineering, Kyushu University, Fukuoka 819-0395, Japan

2. Mine Planning Section, Ministry of Mines, Nay Pyi Taw, Myanmar

3. Department of Mining Engineering, Institute Technology Bandung, Bandung 40116, Indonesia

Abstract: Most of coal is produced from open-cut mines in Southeast Asian countries. However, the conditions of their surface mines are worsening each year: the stripping ratio is increasing, approaching economic ratio and the regulation of environmental protection. To meet the demand for coal, underground mines have to be developed in the near future. Under these circumstances, the development of new coal mines from open-cut highwalls are being planned in Southeast Asian Countries. Moreover, some of the Southeast Asian mines have thick coal seams. However, if the conventional mining systems and designs introduced in US, Australia and European Countries are applied, several geotechnical issues can be expected due to the mines' weak geological conditions. From these backgrounds, this paper proposed a punch multi-slice mining system with stowing for thick coal seam under weak geological conditions and discussed its applicability and suitable design by means of numerical analysis.

Key words: Punch multi-slice longwall mining, thick coal seam, weak strata, stability of highwall.

1. Introduction

The surface mining method is generally considered to be more advantageous than the underground method, especially in recovery, grade control, production capacity, economics, flexibility, safety and working environments. Therefore, the surface mining method is common in major coal producing countries [1, 2]. Most of coal is produced from open-cut mines in Southeast Asian countries. However, the conditions of their surface mines are worsening each year: the stripping ratio is increasing, approaching economic ratio, the regulation of environmental protection, and poor infrastructure for coal from inland mining areas [3]. To meet the demand for coal in Southeast Asian Countries and the rest of the world, underground mines have to be developed in the near future. Under these circumstances, the development of new coal mines from open-cut highwalls are being planned in several

mines in Southeast Asian Countries including Thailand, Indonesia, etc. Moreover, some of the Southeast Asian mines have thick coal seams [4, 5]. However, if the conventional mining systems and designs introduced in US, Australia and European Countries are applied, several geotechnical issues can be expected due to the mines' weak geological conditions [6]. From these backgrounds, a punch multi-slice top coal caving method with stowing was proposed as a mining system for thick coal seam and weak geological conditions.

This paper discusses the applicability of punch multi-slice top coal caving method to the mines in South-East Asian Countries and its suitable design and measures by means of numerical analysis.

2. Punch Mining System

One of the major mining system for final highwall of surface coal mine is highwall mining system. Conventional highwall mining systems extract coal with an auger machine or continuous miner. However, less coal recovery is a problem in these systems,

---

Corresponding author: Takashi Sasaoka, assistant professor, research fields: ground control in mining, blasting and mining system. E-mail: sasaoka@mine.kyushu-u.ac.jp.

because many coal pillars have to be left in order to maintain the highwall/mined openings stability and the mined length is limited by the inherent characteristics of the systems. Considering these issues, the introduction of underground mining systems is also an alternative. The punch mining system is not a new concept [7]. The first punch mining system using an Archveyor system was proposed and tried in the US as shown in Fig. 1. However, this mining system has to leave a lot of coal as pillars.

Rapid access punch longwall mining has been practiced in Australia. Australia's first punch longwall mining operation commenced in the late 1990s using conventional longwall equipment to mine coal from blocks developed directly from an open-cut final highwall [8]. Fig. 2 shows the schematic of punch longwall mining system.

Beltana is a highwall access longwall punch mine, which achieved its first full year of operation in 2004, producing 6 Mt (ROM: Run-of-Mine) coal. It is considered to be the most cost-efficient longwall operation in Australia [9]. The advantages in this system of mining are: high productivity; the system requires no transport, conveyor drifts, shafts, complex ventilation systems or main headings as in conventional
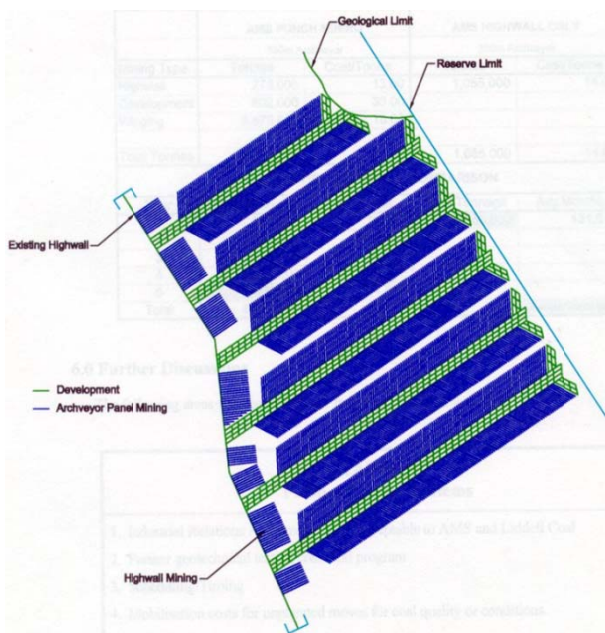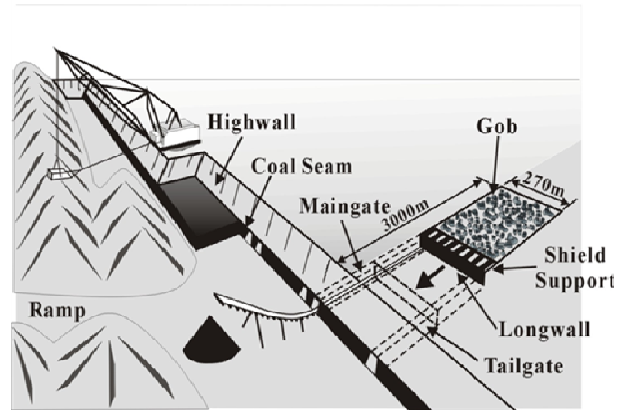

Fig. 2   Punch longwall mining system.

underground mining methods, hence this benefit provides cheaper, faster, simpler access and commencement of longwall mining. However, it is required proper mine planning and mine design to retain and maintain the open cut surface infrastructure throughout the life of underground operations. Due to its advantages of high production capacity and productivity, and competitively lower cost than highwall mining system, this system is expected to be increasingly implemented in Australian coal mines. However, the design and the ground behavior around the mining panel/face and its impact of the stability of slope and the mining operation in weak geological condition have not been made clearly.

3. Multi-slice Top Coal Caving Method with Stowing

While considering the situation of Southeast Asian mines, an applicability of highwall mining systems are less potential due to their limitations in penetration lengths. It is seen that punch highwall mining systems may be considered for the mines. However, as for extraction of the thick coal seam, it must be mined by dividing the seams into multi-slicing. However, when multi-slicing method is applied, the ground behavior around the mining panel/face and their impact of the stability of slope and the mining operation have not been made clearly yet. In case, the ground control issues such as highwall instability can be expected if a conventional thick seam mining method is introduced.

Fig. 1   Punch mining system.

A new multi-slice top coal caving mining method based on the concept of punch longwall and top coal caving methods is proposed. The concept of the new multi-slice top coal caving mining method is illustrated in Fig. 3. First, the coal seam is developed along the mine roof with conventional cut. Then stowing material is injected into gob area in order to have better mine roof condition. After the stowing material is consolidated, the next slice is begun by leaving appropriate thickness of coal parting beneath the first slice and it is recovered by applying a top coal caving method in the second slice. After the second slice is extracted using a top coal caving method, stowing material is injected into the gob area in the second slice. Next slices are also extracted by applying a top coal caving method and stowing is conducted after each slice is mined out and mining and stowing are repeated until the whole coal seam is mined out as the same manner. By applying this method, the number of slices required for the extra-thick coal seam and the burden for excessive costs for development of gate roads required for extra-thick seam can also be overcome compared with an application of the conventional multi-slice mining method. It will be also useful to reduce the impact on ground/slope due to extraction of extra-thick coal seams and can also be useful to minimize the amount of waste rocks managed on surface.

4. Numerical Analysis

When an underground mine is developed from an open-cut highwall, the design of panels and safety pillars such as boundary pillar and inter-panel pillar in the transition area have great influenced on the highwall stability as well as the amount of resource recovery around the final highwall. If the pillar and panel sizes are inadequate, it is possible for slope instability or sliding of slope due to insufficient support to the highwall. On the other hand, if the pillars are over-sized, the amount of resource recovery around the highwall will be decreased. Therefore, careful planning

and designing of panels and pillars around the final highwall. In order to make the criteria for the applicability and the design of a punch multi-slice top coal caving method around the final highwall, the response of ground/slope under weak geological conditions and different operational conditions are investigated by means of FLAC3DVer.5.

4.1 Numerical Model

In surface mining, as the bench design is usually based on economic reach of the mining equipment used in the mine, characteristics of deposit, production strategy and geological and geotechnical condition of the mine. In this study, therefore, the following assumptions are made based on the typical bench design for open-cut coal mining practices [10]. The height of the each single bench is designed as 20 m, and the bench slope angle is 65 degrees. The width of the bench is set as 36 m whereas the safety berm is 6 m wide in the models. The angle of overall slope is 37 degrees. The geometry, meshes and group of zones and dimension of the 200 m deep pit model employed in the analyses are illustrated in Fig. 4. In this study, mechanical properties of rock obtained from one Indonesian surface coal mine are used in this study as represented in Table 1.

The design of panels and pillars in transition area from surface to underground mine for thick seam under weak and strong geological condition are discussed. Due to the advantages of highest efficiency
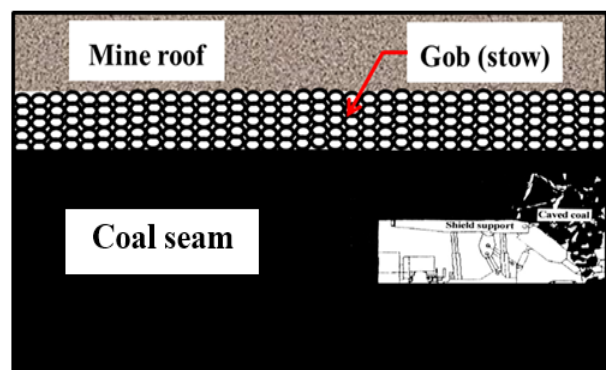

Fig. 3 Concept of multi-slice top coal caving with stowing method (longwall mining system).
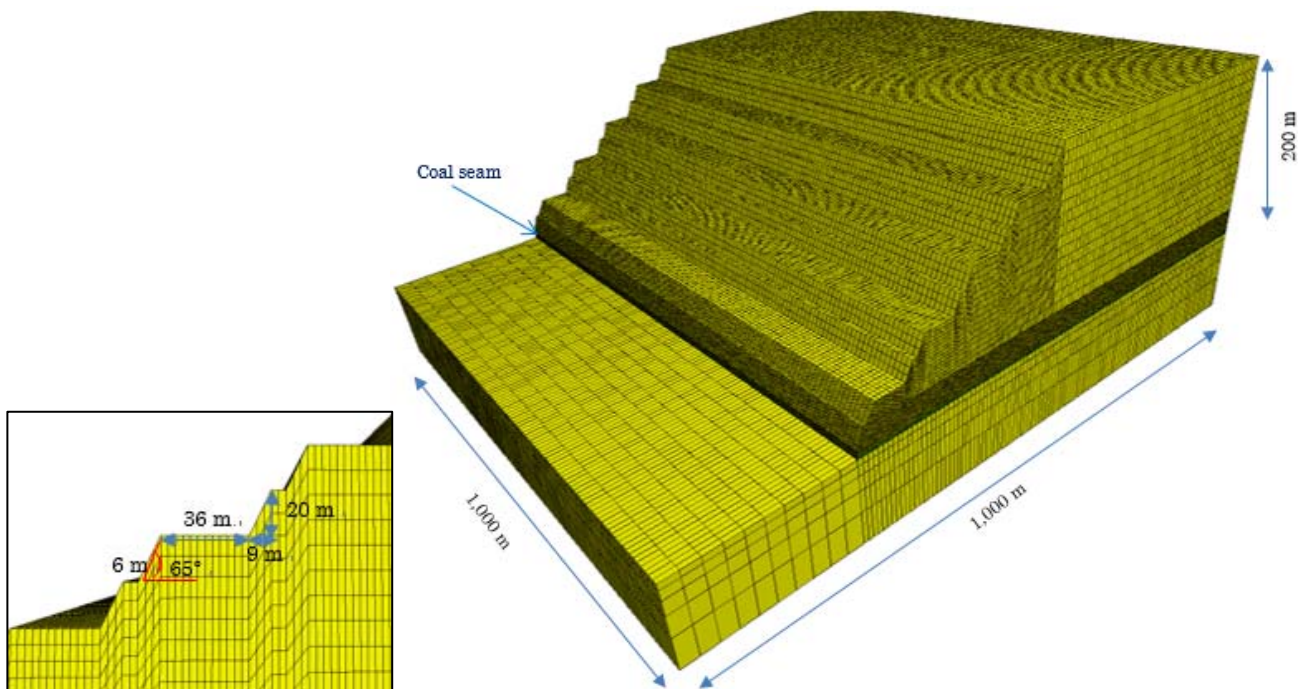
Fig. 4   Numerical model (Pit depth = 200 m).

Table 1   Mechanical properties of rock mass and coal used in this analyses.

	Rock mass	Coal
Density (kg/m^3)	1,950	1,430
UCS (Uniaxial compressive strength) (MPa)	11.36	5.0
Bulk modulus (MPa)	6.67×10^3	3.79×10^2
Shear modulus (MPa)	4.0×10^4	1.95×10^2
Tensile strength (MPa)	0.1	0.1
Cohesion (MPa)	1.75	0.5
Friction angle (deg.)	25	22.3

and productivity among the methods available for thick seam, a longwall top coal caving method is primarily considered in this study. In longwall top caving practices, although the method allows for more than 10 m thick seam in one pass and up to 80-90% recovery of additional coal, coal recovery is less than expected in practical situation due to coal seam and strata conditions, about 70-80% of coal can be recovered in practical situation. Operational issues also limit top coal recovery and can often account for a greater percentage of the reduce recovery than geological conditions alone. In this study, therefore, two slice system is considered for the 10 m thick coal seam, where the first slice is cut conventionally and next slice

is extracted by top coal caving method. Basically, the height of mining for conventional cut for the first slice was considered as 3 m and next slice is set as 7 m, where 3 m thick of coal is cut along the floor of coal seam and 4 m thick of coal is recovered. The scheme of multi-slice top coal caving mining method performed in the analyses is illustrated in Figs. 5a-5b.

The panels and pillars were initially designed based on the results of preliminary analysis that the conventional longwall mining system is applied for the extraction of 3 m thickness of coal under weak geological condition. The panel of 100 m width and the inter-panel pillar of 60 m width are initially taken and the ground behavior is investigated. The boundary pillar of 100 m width for 200 m and 300 m deep pit and that of 150 m width for 400 m deep is initially taken. Layout of the initial mining panel is shown in Fig. 6.

4.2 Results and Discussions

4.2.1 Punch Multi-slice Longwall Mining System without Stowing System

Figs. 7a-7b and 8a-8b show failure states and contours of induced displacement after extracting second slice in
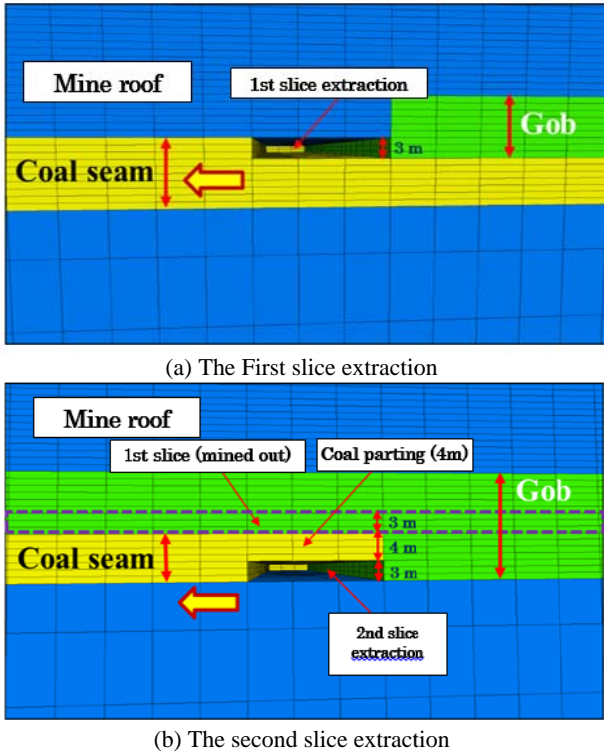
(a) The First slice extraction

(b) The second slice extraction

Fig. 5   Scheme of multi-slicing performed in the analyses (without stowing).
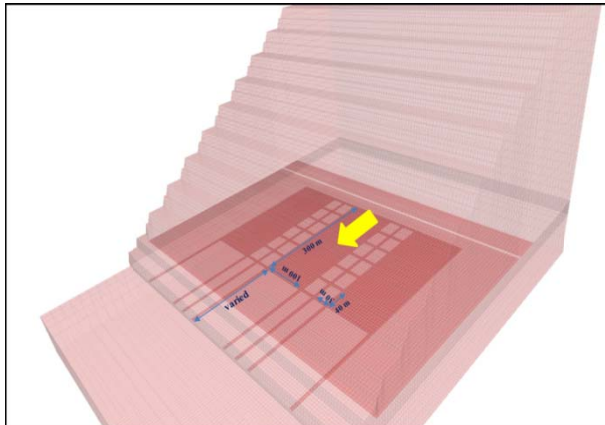

Fig. 6   Layout of panel modelled in the analyses.

200 m and 300 m deep pit slopes, respectively. In the case of 200 m pit depth, as the displacement at the slope is observed 6.5-7 cm in maximum and the boundary pillar is also in stable condition. Therefore, it can be said that the stability of overall slope can be maintained under these panel and pillar designs. On the other hand, in the cases of 300 m pit depth, even though the vertical displacement at the slopes is about 6.5-7 cm in both cases, large failures are occurred at the boundary pillars. In this situation, if the condition at the

toe of the slope is worsen and the pillar is failed, the whole slope instability and/or slide would be occurred. Consequently, the widths of boundary pillars are increased into 200 m in the cases that the pit depth is larger than 300 m.

Figs. 9a-9b and 10a-10b show the failure states and contours of displacement in the cases of 300 m and 400 m deep pits. In the case of 300 m deep pit depth, the condition of boundary pillar can be improved and the slope can be maintained. On the other hand, in the case of 400 m deep pit, as the boundary pillar is still failed and the large displacement can be recognized in the slope, the stability of overall slope still cannot be maintained. Therefore, the ground behavior by modeling with larger inter-panel pillar and smaller panel width is discussed in the case of 400 m pit depth.

The width of inter-panel pillar is increased from 60 m to 100 m and the width of panel is decreased from 100 m to 60 m. Fig. 11 illustrates the layout of panel and Figs. 12a-12b shows the failure states and contours of displacement in this conditions. It is found that the displacement at the slope is decreased from 4.5-5 cm
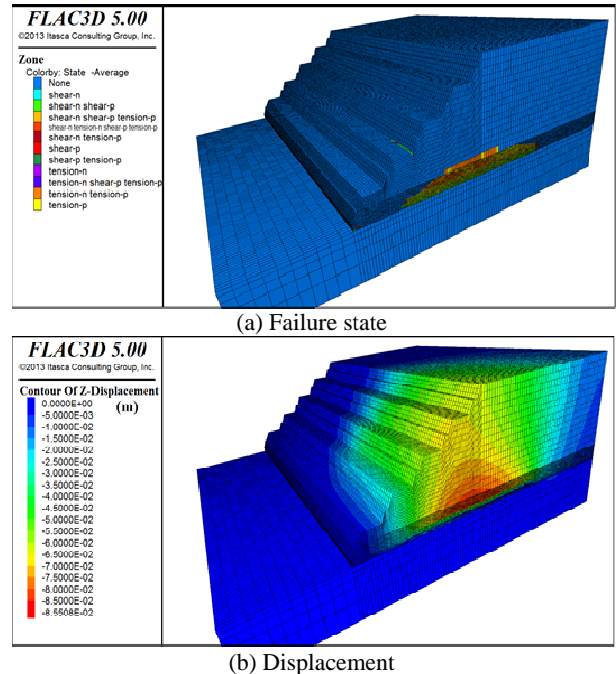

(a) Failure state

(b) Displacement

Fig. 7   Failure states and contours of displacement after extracting 2nd slices in 200 m deep pit slope (boundary pillar width = 100 m, inter-panel pillar width = 60 m, panel width = 100 m).

(a) Failure state

(b) Displacement

Fig. 8   Failure states and contours of displacement after extracting 2nd slices in 300 m deep pit slope (boundary pillar width = 100 m, inter-panel pillar width = 60 m, panel width = 100 m).

(a) Failure state

(b) Displacement

Fig. 9   Failure states and contours of displacement after extracting 2nd slices in 300 m deep pit slope (boundary pillar width = 200 m, inter-panel pillar width = 60 m, panel width = 100 m).

into 3.5-4 cm. In addition, the failure condition of boundary pillar is improved and its stability can be

maintained. However, a plenty of coal have to be left in order to maintain the stability of slope in the case of 400 m deep pit.

4.2.2 Application of Stowing System

According to the results discussed above, it is found that punch multi-slice top coal caving method can also be applicable around the final highwall by a proper panel and pillar design. However, since the large amount of coal have to be left as the pillars, coal

(a) Failure state

(b) Displacement

Fig. 10   Failure states and contours of displacement after extracting 2nd slices in 400 m deep pit slope (boundary pillar width = 200 m, inter-panel pillar width = 60 m, panel width = 100 m).

Fig. 11   Layout of panel modeled in the analyses for 400 m deep pit slope (boundary pillar width = 200 m, panel width = 60 m, inter-panel pillar width = 100 m).
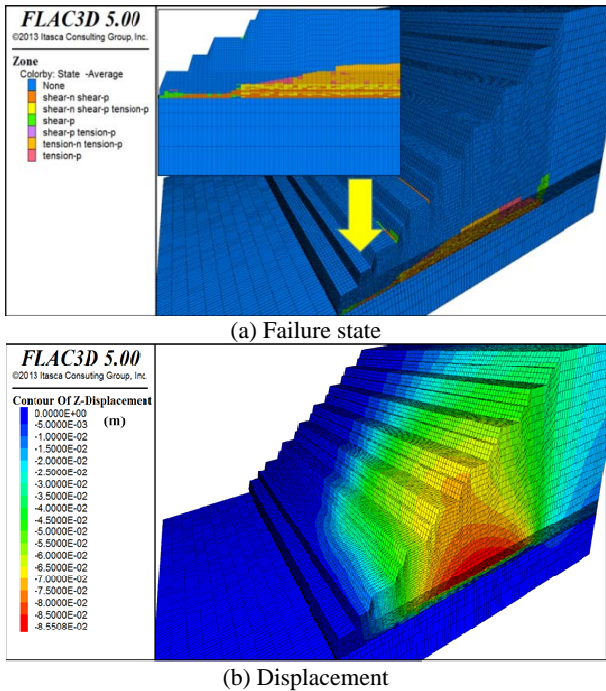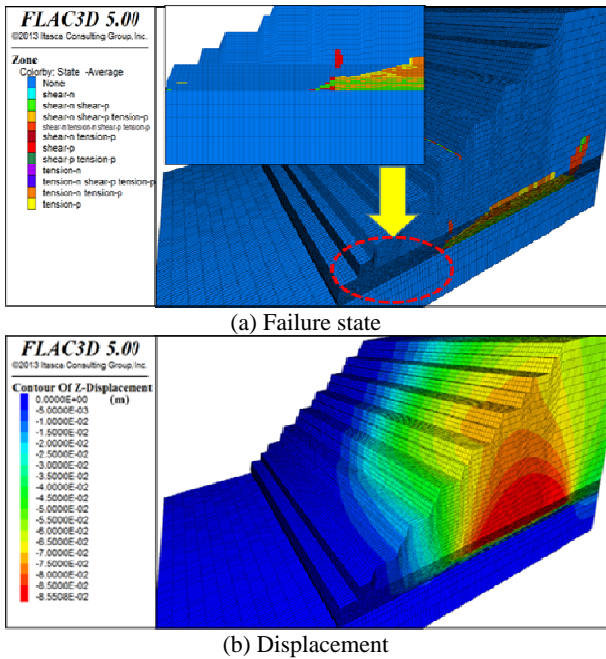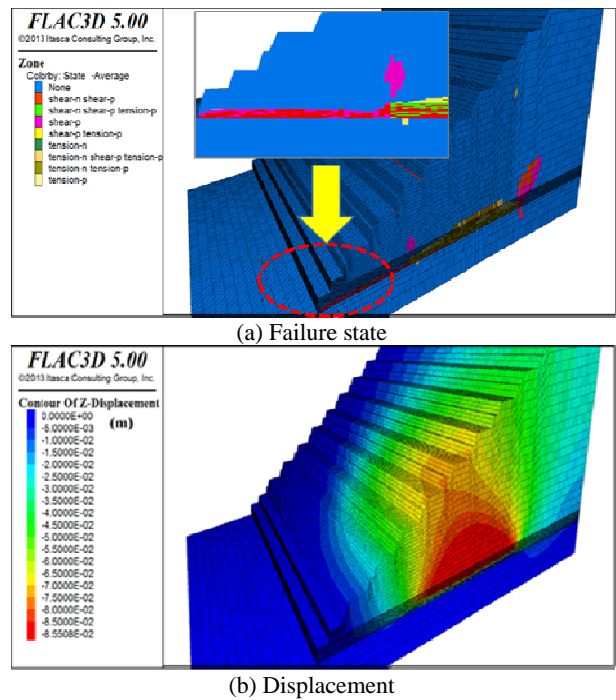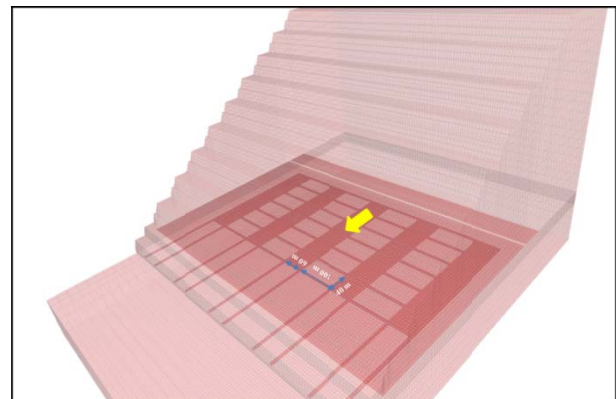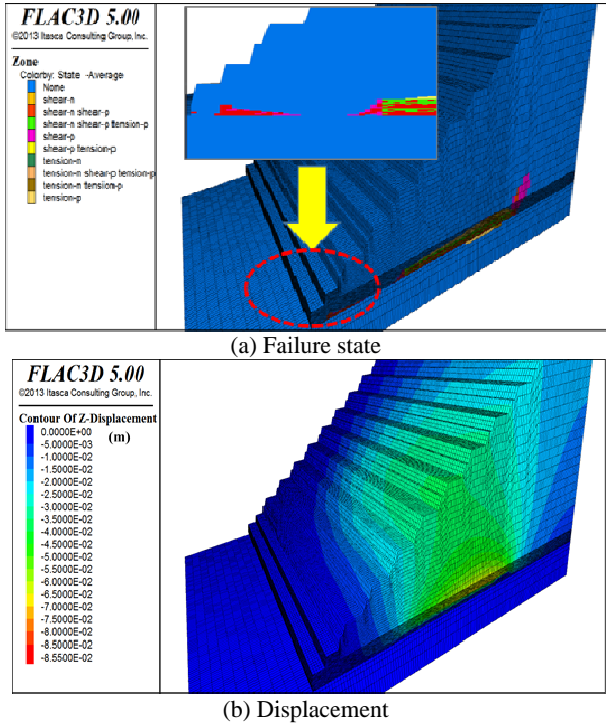
(a) Failure state

(b) Displacement

Fig. 12   Failure states and contours of displacement after extracting 2nd slices in 400 m deep pit slope (boundary pillar width = 200 m, inter-panel pillar width = 100 m, panel width = 60 m).

(a)The First slice extraction
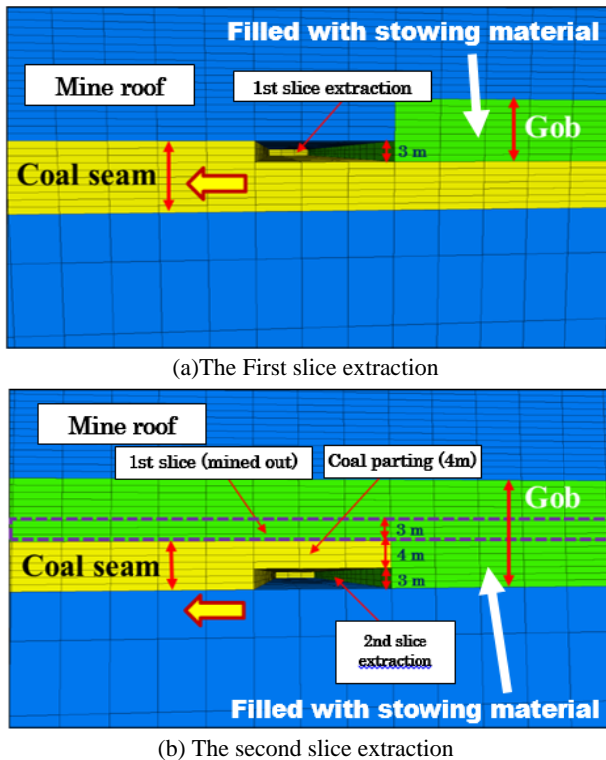

(b) The second slice extraction

Fig. 13   Scheme of multi-slicing performed in the analyses (with stowing).

recovery will be decreased. Therefore, the application of multi-slice top coal caving in conjunction with stowing method is investigated and discussed.

The first slice is also extracted with conventional cut with 3 m mining height and stowing is injected into the gob immediately. After extracting and stowing the first slice, next slice extractions were conducted by applying longwall top coal caving method with leaving top coal 4 m thickness and cutting height of 3 m in second slice. Stowing is followed after each face advance as the same manner as in the first slice (see Figs. 13a-13b).

In the analyses, the panel and pillar sizes are initially designed as 100 m and 60 m as shown in Fig. 6 and the boundary pillar width is taken as 100 m for 200 m deep pit, whereas 200 m for 400 m deep pit. A flyash cement is taken as the slurry stowing material.

The mechanical properties of this stowing material used in the analyses are: density $1,000 \, kg/m^3$, Poisson's ratio 0.23, Young's modulus 617 MPa, tensile strength 0.5 MPa, cohesion 0.5 MPa, friction angle 26 degrees, respectively.

At first, the performance of stowing is investigated in the 200 m deep pit. Fig. 14 shows failure states and contours of displacement after extracting second slice with multi-slice top coal caving with stowing. It is found that failure zone around the mine roof becomes to be small dramatically and the displacement is decreased from 6.5-7 cm into 2.5-3 cm. Since the subsidence at the slope is very small, the subsequent effect of subsidence at the slope such as failure, crack or sliding of slope will not be expected.

Figs. 15a-15b show failure states and contours of displacement after extracting second slice in 400 m deep pit. No failures are found in the boundary pillar and the displacement at the slope is small and about 3-3.5 cm after stowing even the panel size increases from 60 m to 100 m and the panel size increases from 60 m to 100 m. Hence, the application of stowing system can not only improve the stability of slope and but also increase coal recovery.
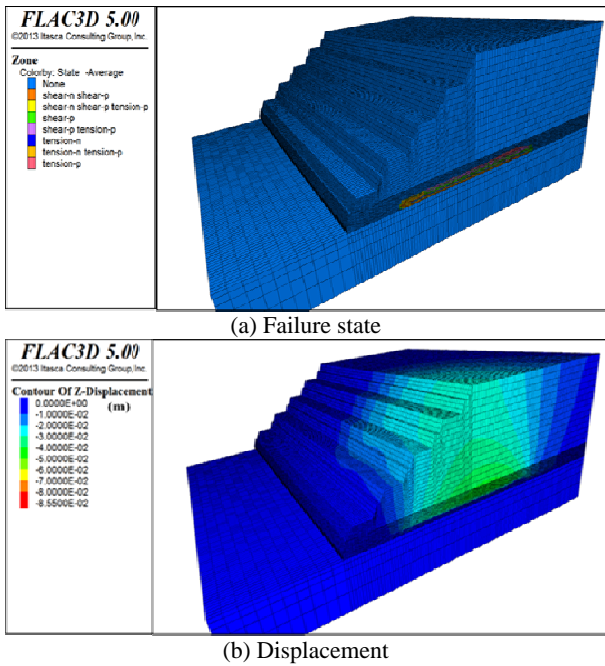
(a) Failure state

(b) Displacement

Fig. 14   Failure states and contours of displacement after extracting 2nd slices in 200 m deep pit slope (boundary pillar width = 100 m, inter-panel pillar width = 60 m, panel width = 100 m).
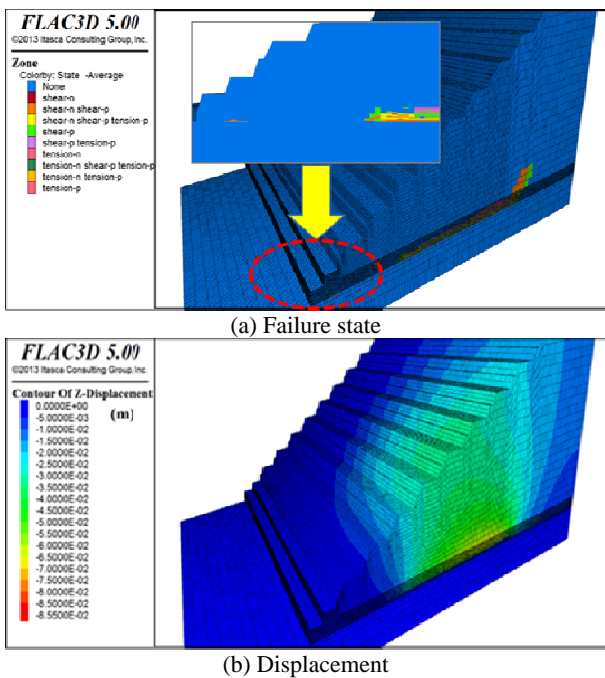

(a) Failure state

(b) Displacement

Fig. 15   Failure states and contours of displacement after extracting 2nd slices in 400 m deep pit slope (boundary pillar width = 200 m, inter-panel pillar width = 60 m, panel width = 100 m).

From the above discussions, it can be concluded that the stowing is effective method for prevent the failure

of pillars and control the displacement at the slope. In comparison with previous results without stowing, the boundary pillar width 200 m need to be left in order to be in stable and to have safe operation in 300 m deep pit. If stowing is applied, the boundary pillar width of 100 m is enough although the size of panel and inter-panel pillar sizes are the same. In 400 m deep pit, even though the boundary pillar of 200 m width still has to be left, the panel width to inter-panel pillar ration can be increased. For example, in the case of 400 m deep pit, the ratio of the width of panel to inter-panel pillar is approximately 0.60 : 1 when without stowing. However, if stowing is applied, the ratio of the width of panel to inter-panel pillar is approximately 1.67 : 1 when stowing is applied. In addition, since longer extraction length can be set, the productivity will also be higher.

5. Conclusions

The applicability of punch multi-slice top coal caving method for thick coal seams in different pit depths under weak geological conditions and appropriate design of boundary pillars, inter-panel pillars and panels are investigated and discussed in this paper. Moreover, the application of multi-slice top coal caving in conjunction with stowing for weak and thick seam is proposed and discussed in order to increase the coal recovery and improvement of stability of slope. It is found that stowing is quite effective to prevent the pillar failure and to control the stability and subsidence at the slope. As the results, the coal recovery can be improved.

However, in order to develop the appropriate design of punch multi-slice top coal caving method under weak geological condition, the more study have to be conducted including the control of top coal caving, the stowing material, sizes of panel/pillar, mining sequence, etc.

References

[1]   Oya, J., Shimada, H., Sasaoka, T., Ichinose, M., Matsui, K., Pertiwi, R., and Fajrin, A. M. 2009. "Fundamental Study

on AMD-prevention by Compacted Waste Rocks at Berau Coal Mine, Indonesia." In *Proceedings of the 2nd International Symposium on Novel Carbon Resource Science*, IV19-IV24.

[2] Inoue, N., Hamanaka, A., Matsumoto, S., Shimada, H., Sasaoka, T., and Matsui, K. 2014. "Effective Assessment Methods of Soil Erosion Control in Indonesian Open Pit Mine." In *Proceedings of 18th Conference on Environment and Mineral Processing*, 221-7.

[3] Matsui, K., Sasaoka, T., Shimada, H., Furukawa, H. Takamoto, H., and Ichinose, M. 2010. "Some Consideration in Underground Mining Systems for Extra-thick Coal Seam." In *Proceedings of the 3rd International Symposium on Mineral Resources and Mine Development*, 355-68.

[4] Hamanaka, A., Sasaoka, T., Shimada, H., Matsui, K., and Takamoto, H. 2011. "Application of Punch Mining System to Indonesian Coal Mining Industry." In *Proceedings of the 20th International Symposium on Mine Planning and Equipment Selection*, 187-97.

[5] Shibata, S., Lin, N. Z., Shimada, H., Hamanaka, A., Sasaoka, T., Matsui, K., and Lawowattanabandit, P. 2013. "Preliminary Study on Design of Longwall Mining from Final Highwall at Mae Moh Lignite Mine in Thailand." In *Proceedings of the 22nd Mine Planning and Equipment Selection*, 227-34.

[6] Sasaoka, T., Shimada, H., Takamoto, H., Hamanaka, A., and Matsui, K. 2012. "Development of Underground Coal Mine from Open Cut Highwall in Indonesia." In *Proceedings of 5th International Symposium on High Performance Mining*, 495-510.

[7] Robertson, B. W., O' Regan, G., and McKew, M. 1988. "Longwall Punch Mining from Open Cut Highwalls." In *Proceedings of the AUSIMM Illawara Branch 21st Century Higher Production Coal Mining Systems*, 215-20.

[8] Macdonald, S., and Hill, D. 2008. "Practical Strata Management, Beltana No. 1 Mine, Australia." In *Proceedings of 27th International Conference on Ground Control in Mining*, 275-83.

[9] Hill, D., and MacKinnon, M. 2011. "Case Study of Roof Behavior and Conditions for Longwall Face Recoveries at Beltana No. 1 Mine, Australia." In *Proceedings of 30th International Conference on Ground Control in Mining*, 265-70.

[10] Hem, P. 2012. "Pits & Quarries." In *Techno Mine*. Accessed October 25, 2014.http://technology.infomine.com/reviews/pitsandquarries/welcome.asp?view=full.

WHR (Waste Heat Technology) Method in Tri-generation Model

Imrich Discantiny

COMTHERM s.r.o., Palatínova 39, Komárno 94501, Slovak Republic

Abstract: This paper is focused on description of cool production in using WHR (Waste Heat Technology) Technology—a new method of centralized production of heat by using the waste heat from generated exhaust gas, which has been in 2009 developed and operated by companies HELORO s.r.o. and COMTHERM s.r.o.

Key words: NG (natural gas), GB (gas boiler), CHP (combined heat & power), CHPC (combined heat & power & cool), CGU (co-generation unit), ABSU (absorption unit), TC (thermal condenser), HE1, HE2 (heat exchanger).

1. Background/Introduction

This Abstract is focused on description of cool production in using WHR (Waste Heat Technology) Technology—a new method of centralized production of heat by using the waste heat from generated exhaust gas, which has been in 2009 developed and operated by companies HELORO s.r.o. and COMTHERM s.r.o. In 2013, the technology was combined with the utilisation of renewable energy sources—heat emissions from surrounded facilities, geothermal well, located on the operations site, as well as installed solar collectors. As of 2014 the companies focused on the research and development in the field of tri-generation , i. e. the highly efficient combined production of CHPC (electricity, heat and cooling), connecting a hot water absorption chiller unit to CHP (combined heat & power) technology in combination with WHR technology. The new advanced and progressively developing processes in the segment of highly efficient combined electricity (CHP) and heat production enhance the living standard, and provide a higher comfort of living in apartment, administrative and production buildings and facilities. Simultaneously with such growing segment grows the

Corresponding author: Imrich Discantiny, Dipl. Ing., research field: renewable energies. E-mail: discantiny@comtherm.sk.

importance of a flexible production of cold.

2. Problem

Operation of installed high efficient CHP units must be mostly interrupted during the summer period.

Our generation have more actual environmental problems, i.a.:

• To fix climate change;

• To cut greenhouse gases by 60% by 2050;

• To build a pollution-free heat & power plants;

• To sort out a new way of getting energy;

• The needs in the cool production are continuously growing;

• There is no other possible way of doing that except through renewables. So we seek new;

• Environmental solutions and alternative energy sources.

3. WHR Technology Description

The technological WHR solution depends on the method and system of flue gas processing for the flue gas that is generated through the combustion of gaseous fuel (NG (natural gas), methane, biogas, and geothermal gas) in the heat source. The solution defines more effective and non-traditional usage of gaseous fuel for heating, where the flue gas is further processed in order to extract from it additional usable

heat, with the potential subsequent elimination of CO_2 from it in the separation module.

3.1 Current Deployment of Condensing Boilers in Operations

Gas boilers use the condensation heat, and they operate at the lower interval of heating medium temperatures (35 °C-40 °C) in the recurrent sleeve and significantly lower than the dew point temperature, which is approximately 57 °C. Hence such solution is not applicable in case of a central heating, where the heat production plant operates with a much hotter heating medium in the recurrent sleeve (55 °C), and at such temperature one cannot reach the condensation of the flue gas (neither in case of heat exchangers with large surfaces) through the direct deployment of a recurrent sleeve. The model of thermal condensers connection set-up, which drains the flue gas from the heat source, has an additional disadvantage in that the flue gas cannot be cooled down below the recurrent sleeve temperature, which thus prevents the effective condensation of water vapours.

The partial condensation starts at the flue gas temperatures below 70 °C, however an efficient use of the specific latent heat starts only at the temperature below dew point. Cooling of the flue gas below dew point temperature causes condensation of the water vapour and the release of condensation heat. The aim of the essential WHR technology model is to provide a very intensive flow of water vapour condensation. The more efficient is the cooling of flue gases and the course of condensation, the higher and the quantity of residual heat that could be used for heating; whereas the higher degree of flue gas cooling, the more efficient will be the separation of CO_2 in the separator device. [1]

The processing of the flue gas waste heat using WHR technology eliminates the shortcomings of the existing status of hardware, where the heat source transmits heat to the heating medium in the exit sleeve, and the heating medium returns through the recurrent sleeve back to the heat source.

3.2 WHR Method in Tri-generation Model

The boiler room set-up clearly shows that the natural gas medium is carried into the cascade-connected set of heating boilers, and into the heat source No. 2—CGU (co-generation unit), which generates with added value the required electric energy needed for the operation of the boiler-room equipment, including the operation of the heat pump drive (see Fig. 1).

3.2.1 HE1 (Heat Exchanger)

The flue gas generated through the combustion of gaseous fuel in the heat sources (in the heating boiler/120 °C and in CGU/170 °C) are through the joint flue gas piping connected to the HE1 (of gas/liquid type), where takes place the transfer of heat into the heating medium at temperatures above the recurrent sleeve temperature. The HE1 act as a source of heat/70 °C for a secondary circuit flowing to the boilers, which acts as pre-heating module for the recurrent circuit (from the temperature 70/60 °C).

3.2.2 TC (Thermal Condenser)

TC is a specific type of heat exchanger, which is adjusted to cope with the waste heat from the flue gas together with the condensation heat from the water vapours.

In the course of this process, the flue gas cools down to a temperature that is lower than the flue gas dew point, and at the same time lower than the temperature within the heating medium in the recurrent sleeve. At the same time, the cooling circuit of the thermal condenser will not be directly interconnected with the heating medium recurrent sleeve. [1]

The process of cooling down to the temperature/25 °C is permanent, and it is accompanied by a high degree of water vapour condensation, which causes drying of the flue gas, and it has three, mutually combinable advantages—the process is accompanied by the release of condensation heat, and by the release of H_2O with a significant share of NO_x emissions into the sewage, and at the same time it is possible to arrange at the next downstream stage a separation of CO_2 in the separation equipment.
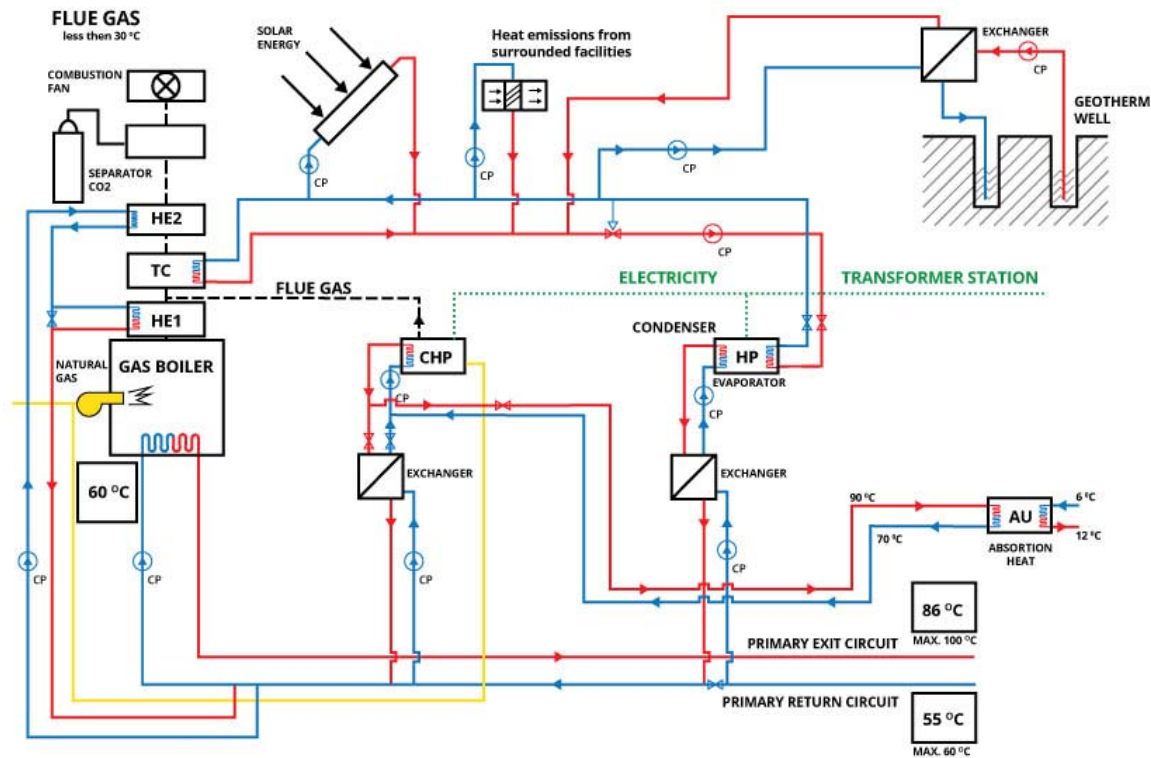
Fig. 1   General scheme of the boiler house.

3.2.3 HP (Heat Pump)

The source of heat for the heat pump is the TC (thermal condenser), connected to a separate circuit, within which is the low potential heat pumped to a higher temperature, utilisable in the heating system. Since the initial exit temperatures 10/31 °C would normally not be suitable for start-up of the HP, this closed circuit will be complemented by adding a 3WV (three-way valve) and a CP (circulating pump), which would allow regulation of the heat-carrying medium input also from other sources of low-potential heat (solar panels, well, ...). Temperature falling gradient directly at the entry to this heat pump circuit is 10/18 °C, and in case of such temperatures, we see the benefits of the proposed connection set-up, when the TC cooling sleeve is fed with the 10 °C heat-carrying medium, which guarantees a sufficient temperature gradient that cannot be reached using a heating medium

with the temperature/50 °C. [1]

In energy sector, owing to their high performance number COP (Coefficient of Performance) (3.8-4.5), the heat pumps are becoming an important technological component, increasing the energy efficiency to more than 100%. In particular, in case of a complex WHR technological system this total efficiency figure reaches 115% (as a mix of 30% power generation efficiency, and 85%—heat production efficiency).

3.2.4 HE2 (Heat Exchanger)

Within the heat exchanger HE2 (of gas/liquid type) takes place the partial pre-heating of cooled liquids (although without NO_x emissions) to a temperature tightly above the dew point, in order to avoid an unwanted condensation of water residues in the chimney liner.

Substantial degree of CO_2 separation takes place in

the separator device, mounted on the extruding part of the heat exchanger HE2, which operates based on the cooling principle. [1]

Unused volume of flue gases (25 °C) is evacuated through flue ventilator in a dry state (approximately 30-40 °C) into the chimney.

3.2.5 Tri-generation, Connection of AU (Absorption Unit) to CHP & HP System

WHR technology operates as a tri-generation involving the process of cooling within the cogeneration unit's heat-generating circuit, which could be arranged in two ways:

Through connection to the heat exchanger in the heat-generating circuit (of liquid/liquid type), with the follow up transfer of heat for pre-heating to the heating medium recurrent sleeve via heat exchanger, at the same time is the CHP unit cooled down.

Through connection of an AU (absorption unit) to the heat-generating circuit, where the produced heat from CGU is effectively converted to cold (6°C-12°C) at the temperature regime 90/70 °C, where as the waste water from AU (40 °C) can be used to effectively pre-heat the water in the hot service water production step.

4. Consumption of Input Energy Carrier and Costs Savings

The Fig. 2 and Table 1 indicate the NG consumption savings of a system, combining CHP simultaneously with heat pumps versus gas-fuelled condensing boiler. [4]

5. Energy Savings Summary

The 60 °C pre-heated medium enters the gas boiler (see Fig. 1). As a simplification we can say that we have saved energy that would be needed to raise the temperature of the heating medium from 55 °C to 60 °C. The Fig. 2 and Table 1 [4] indicate the NG consumption savings of a system, combining CHP simultaneously with heat pumps versus gas-fuelled condensing boiler. The Fig. 3 indicates energy diagram of CHPC (combined heat, power & cool) & WHR energy system. [3]

6. Pay-back Period of Investment

It depends on the existing system, industry segment, and the consumption of heat and electricity. According to our experience, the payback period has never exceeded 4 years.
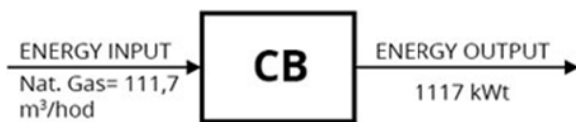
Fig. 2   Comparative diagram of natural gas consumption. [3]
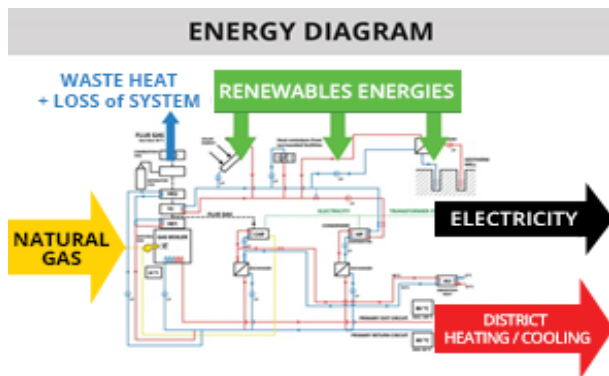
Fig. 3   Energy diagram.

Table 1   Evaluation of Natural Gas Costs Savings. [4]

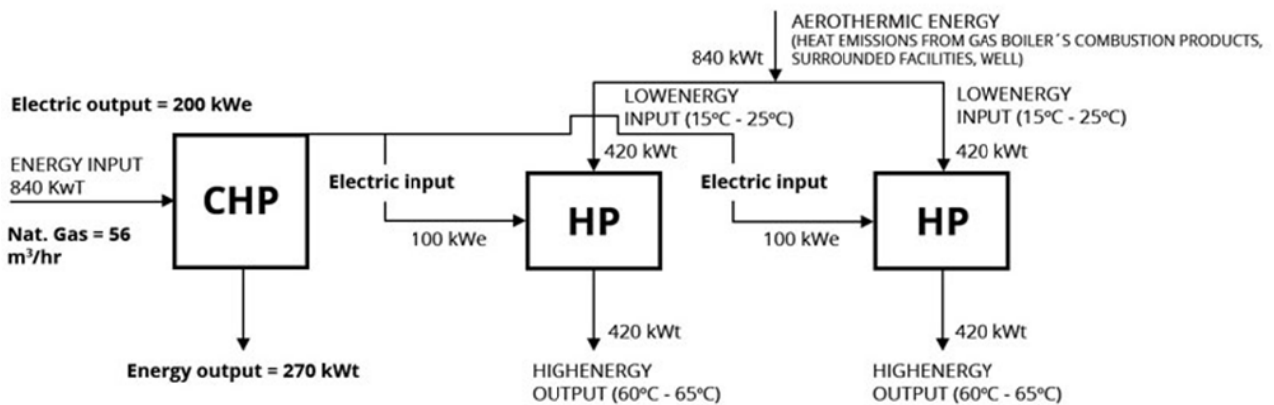|	
Assumed consumption of CB	11,170 m^3
Consumption of combined system CHP & HP	56 m^3/hr
HG saving/hr	557 m^3/hr
Annual NG saving (8000 hr)	445,600 m^3
Financial calculation (approx.)	147,000 eur

7. Conclusions

The industrial applicability of the basic WHR technology model in combination with the absorption cooling is self-evident. Through 3-year operation in real environment in the gas-operated heat plant we have demonstrated the possibility of industrial and recurrent utilisation of waste heat from the heat source-generated flue gas, with the spin-off benefit of separation of NO_x and CO_2 emissions from the flue gas. In addition to a significant environmental benefits the connection set-up has demonstrated also the system's enhanced energy efficiency, and an improved efficiency of the gaseous fuel.

This modification opens new and effective possibilities of enhanced energy efficiency of heat sources with the subsequent reduction of annual operating costs of thermal management of buildings, building complexes etc., since during the summer period all installed technology remains operating.

Tri-generation develops a possibility to reduce the economic intensity of all-season generation of heat and cold. It becomes an actual and attractive technology for the solution of communal needs, which increasingly require more and more of cooling. In addition to standard air-conditioning solutions, nowadays we meet more and more often the engineering networks with complete cold distribution networks, and/or cold distribution piping, either in urban quarters or even in the whole cities. One can assume that in several years the production of cold will become comparable to the production of electricity and heat. The current trend has been caused by several factors:

Development of an architecture with glass-covered facades of new buildings.

Appliances operated in individual rooms generate certain heat output (servers, fridges, as well as other daily appliances)

For these reasons, all around the world, the production of cold marks a fast growth. In addition to standard air-conditioning solutions, nowadays we meet more and more often the engineering networks with complete cold distribution networks, and/or cold distribution piping, either in urban quarters or even in the whole cities.

References

[1] COM-therm, s.r.o., Bratislava/Heloro, s.r.o. *Utility Model 300020 DE 1.* Bratislava: COM-therm, s.r.o., Bratislava/Heloro, s.r.o.

[2] Industrial Property Office. 2011. *The basic Utility Model Nr. SK 6120 Y1.* Slovak Republic: Banská Bystrica.

[3] Discantiny, I. 2014. *WHR Innovative Technology-Intelligent Energies, Gas for Energy.* München: DIV Deutscher Industrieverlag GmbH.

[4] Discantiny, I. 2015. *New Technology of the Use of Waste Heat from Heat Source* (*Nová technológia využitia odpadového tepla*). SLOVGAS: Slovak Gas & Oil Association. (in press)

Author
Imrich Discantiny
Senior Consultant
COM-therm s.r.o.
Heloro s.r.o.
Komárno, Slovak Republic
E-mail: discantiny@comtherm.sk

Gas Ratio Analysis in Hovsan Oil Field

Samir Hashimov

Department of Lithology, Mineralogy and Petrography, The Azerbaijan State Oil Academy, Baku, AZ1010, Azerbaijan

Abstract: Gas Ratio Analysis is best of the analysis in mud logging system which during drilling time is very important for catch formation. This analysis can help geologist that to decide which layers have oil and gas. Also with this analysis, we can compare that wireline jobs has been right place or not. So after calculate ratio analyses, we can put same place then can compare with wireline curves. In that time, we can see that where exactly have oil and gas. With this method, we can reduce cost and we can do safety job. In Azerbaijan Gas Ratio Analysis has been used in Pirsa at Oil field and has been gotten good result after perforation. Now this method use in Hovsan and Zigh oil field by the mudloggers which belong Surachani district.

Key words: Oil, Gas, lithology, wireline, mudlogging.

1. Introduction

Gas readings are most commonly obtained from the mud system by placing a separator or gas trap in the ditch (possum belly) or flow-line. Extracted gas is drawn into the mud logging unit where its contents are measured by a variety of gas detectors; usually a total hydrocarbon detector, a chromatograph, a CO_2 detector and a H_2S detector. Total gas detectors that monitor for nitrogen, various sulfides and hydrogen may also be used. The amount of gas recorded is dependent upon many variables, including:

- Volume of gas per unit volume of formation;
- Degree of formation flushing;
- Rate of penetration;
- Mud density and Mud viscosity;
- Formation pressure;
- Gas trap efficiency;
- Gas detector efficiency;
- Variability of mud flow rate.

Due to the variability of gas analysis they are generally used only in a qualitative manner. Comparisons to other wells can only be down when indications are similar (i.e. between wells drilled by the same rig, with the same gas trap/detector system and similar mud types).

Corresponding author: Samir Hashimov, master, research field: geological prospecting. E-mail: samirleu@mail.ru.

Gas readings are used with reference to a "background level". The gas readings are then displayed graphically on either the mud log and or the geologists mudlog. This allows an easy evaluation of the relative amounts of gas recorded. Contractors usually record total gas as either a percentage, ppm or in the form of gas units. A gas unit may vary from 0.02% to 0.033% depending upon contractor. The use of percent or ppm allows for better comparison between wells and contractors. A understanding of the mud logger's gas detectors is important when reviewing gas data. The equipment between companies does differ. For example, some companies use chromatographs that do not measure the pentanes (C5), which could be important if the geologist is correlating with another mud log containing C5's. Gas detectors may be of two types, an older catalytic variety or the more modern FID (Flame Ionization Detector) type. CCD detectors use a catalysis approach (that is the catalytic oxidation of gas upon a filament in the presence of air), while the FID use flame ionization (the ionization of a sample into charged hydrocarbon residues and free electrons by combustion). The type of equipment used should be known by the geologist as the two methods are affected differently when non-hydrocarbon gases are present. The catalytic detectors upper limit of

sensitivity is approximately 9.5%. At this point not enough oxygen is available for catalysis. A "negative" response occurs in the presence of CO_2, and the detector is affected by large quantities of nitrogen. Variations in temperature also cause a thermal drift of catalytic detectors. FID detectors are not affected by quantities of nitrogen, CO_2 or temperature variations. To assist in post-well evaluation, the Wellsite Geologist should ask the mud loggers to note the type of gas detection equipment on the mud log. In addition, establish with the client how produced gases (i.e. connection and trip gases) are to be reported. For example, they will be reported as percent above background gas or as a total percentage.

1.1 Gas

As mentioned earlier, many factors affect the amount of gas recorded at the surface. Prior to discussing these at length some definitions are necessary.

True zero gas: The value recorded by the gas detectors when pure air is passed over the detection block (generally done during calibration). To ensure a zero mark, the detectors should be zeroed prior to drilling, at casing points, logging points, etc.

Background zero gas: The value recorded by the gas detectors when circulating, off-bottom, in a clean, balanced bore hole. Any gases monitored will be from contaminants in the mud or from gas recycling. This value is the baseline from which all gas readings are referenced for the striplog and mud log, but not plotted on the logs. This value will change with respect to changes in the mud system (adding diesel) and hole size, and should be re-established periodically.

Background gas: This is the gas recorded while drilling through a consistent lithology. It often will remain constant, however, in overpressured formations, this value may show considerable variation. This is the gas baseline which is plotted on the striplog and mud log.

Gas show: This is a gas reading that varies in magnitude or composition from the established background. It is an observed response on the gas detector and requires interpretation as to the cause. Not all gas peaks are from drilled formation, some may occur as post-drilling peaks.

Connection gases: Gas peaks produced by a combination of near-balance/under-balanced drilling and the removal of the ECD (Equivalent Circulating Density) by stopping the pumps to make a connection. They are often an early indicator of drilling overpressured formations. These should be noted, but not included as part of a total gas curve.

Trip Gases: Gas peaks recorded after circulation has been stopped for a considerable time for either a bit trip or a wiper trip. As with connection gases, substantial trip gases can indicate a near balance between the mud hydrostatic pressure and the formation pressure, they should be recorded but not included as part of a total gas curve. Like other logs, the mud log is a depth-related plot displaying certain physical characteristics of the formations being drilled. In the mud log's case, gas curves are changes in the concentration and composition of formation hydrocarbons. Like other logs, there are baselines or thresholds values, from which deviations may indicate significant events. One such baseline is gas present in normally pressured formations. There may be significant contributions by extraneous factors and the baseline itself may vary (in laminated formations it may oscillate to extremes), but it will provide a standard upon which events will be judged. It is essential that absolute magnitude not be the only basis upon which gas show evaluation is made. The magnitude of a gas show is quantitative only to the air/gas sample obtained and measured at the detector. In correlating gas shows between different wells (especially where a change of rig or engineering approach is involved), the major parameters are curve profiles and relative compositions. As with the correlation of wireline logs, care should be taken to

match up overall curve character and not just individual high and low values. Individual values are never reproducible and extremely high values should always be suspect, and are of little "correlative" use. Logs showing a difference of several orders of magnitude in gas concentrations may be easily correlated by overlaying gas curves and recognizing significant peaks or variations in the form of the curve. Similarly, the significant event may be the appearance of a new component or a notable change in the relative concentration of two or three compounds. At no time should the absolute magnitude of a gas show be taken as a basis for any quantitative statement. As stated earlier, no gas show should ever be considered in isolation. Reference should always be made to the preexistent background value. The gas phase at surface may not, and probably will not, have the same composition as the gas phase in-situ. It will nevertheless reflect the overall hydrocarbon composition (i.e. liquid and gas) of the reservoir, and chromatographic analysis can be used by skilled log interpreters as an important key to evaluation. Again, it is not simply the magnitude of gas shows, but their relative composition linked with all other log parameters which is the key factor. In addition to the conventional log presentations of gas show data, certain mathematical treatments are available by mud logging companies as an aid in interpreting gas shows. Although some of these are attempted normalization (adjustments of the Total Gas values for the normalizing of known downhole effects), most are treatments for chromatographic analyses in order to determine characteristic responses typical of known hydrocarbon types.

1.2 Gas Normalization

The quantification of gas shows is unattainable with current mud logging technology. The many in-situ and drilling variables are almost impossible to calculate during initial evaluation. In-situ variables include porosity, relative permeability, gas saturation,

temperature, pressure, solubility and compressibility of the gases. Once penetrated by the drill bit, other variables come into play, such as flushing, drill rate, pump rate, hole size, rock and gas volume, differential pressure and temperature, phase changes and surface losses.

Normalization is the mathematical treatment of parameters affecting gas shows. Attempts have been made to cover all the downhole variables, such as saturation, temperature, pressure, etc. however, for truly accurate results by these methods, wireline log evaluation must be made first to arrive at a "safe" figure. Gas normalization does not try to cover surface losses, due to the great variations in flow-line and ditch geometries, flow rates and gas trap efficiencies (though studies have been made to determine gas trap efficiency). The most common form of normalization involves correction for drill rate, hole size and pump rate because these parameters are continuously monitored while drilling and can be immediately entered into normalization equations.

2. Materials and Methods

2.1 Correlation

The comparison of relative concentrations of the various hydrocarbons seen in a chromatogram (C1-C5) often has diagnostic value in qualitatively estimating the type and quality of a petroleum reservoir. Such a comparison has also been useful in stratigraphic correlation, where a distinct and characteristic hydrocarbon boundary may be recognized, even when no lithological facies boundary is evident. The study of relative concentrations of light alkanes has been done by various people to evaluate maturity levels and migration modes of petroleum reservoirs. Studies of n-heptane and iso-heptane ratios have been conducted to determine maturity and thermal history classifications of petroleum. Ratio studies of C2-C4 and especially the butane isomers have been used to determine the effect of diffusion in primary migration and the possible maturity trends shown by these

studies. These studies, however draw on data not readily available in normal wellsite logging, and practically all gas ratio studies performed at the wellsite are used to determine the type and quality of petroleum reservoirs. Such studies are mathematical treatments of the hydrocarbon species (C1-C5) using relative concentrations such as C2/C1, C3/C1, etc. Plots from these studies will often yield distinctive "character" or "events" not always immediately evident from the chromatogram itself. Two such ratio methods used are the "Rectangular Plot" and the "Triangular Plot". Though originally designed for steam-still reflux mud or cutting samples, then have been adapted for gas trap readings.

When using either plot, the following corrections must be made:

• Removal of all contamination gas readings, such as diesel, trip gas, connection gas, recycled gas (see Table 1);

• Correction for background gas. The relative concentrations must be read above background gas;

• More than one reading must be done to have any interpretative value.

2.2 Rectangular Plots

The rectangular plot uses the ratios C1/C2, C1/C3, C1/C4 and C2/C3 (or C1/C5) and plots the results on a semi-logarithmic grid (see Fig. 1). Values of these ratios are allocated to potential productivity, where:

Several "rules of thumb" for the rectangular plot are:

• Productive dry gas zones will yield mainly (or only) methane. However, abnormally high ratios may indicate gas in solution in a water zone;

• If C1/C2 falls in the oil section, but C1/C4 is high in the gas section, the zone may be non-productive;

• If any ratio is lower than the preceding ratio, the zone is probably nonproductive;

• If C1/C4 is lower than C1/C3, the zone is probably water wet.

When plotted, the results tend to be in conclusive and a careful review of all log information can yield a more definitive evaluation. In practice, this type of plot can be useful as an illustrative tool and as one component in a complete evaluation.

2.3 Triangular Plots

The triangular plot (see Fig. 2) requires the calculation of the ratios C2, C3 and nC4 to the total of all gases detected (expressed as a percentage). Lines representing those percentages are then drawn on a triangular grid. As with the rectangular plot, all gas percentages are taken above background.

Table 1 Gas relations.

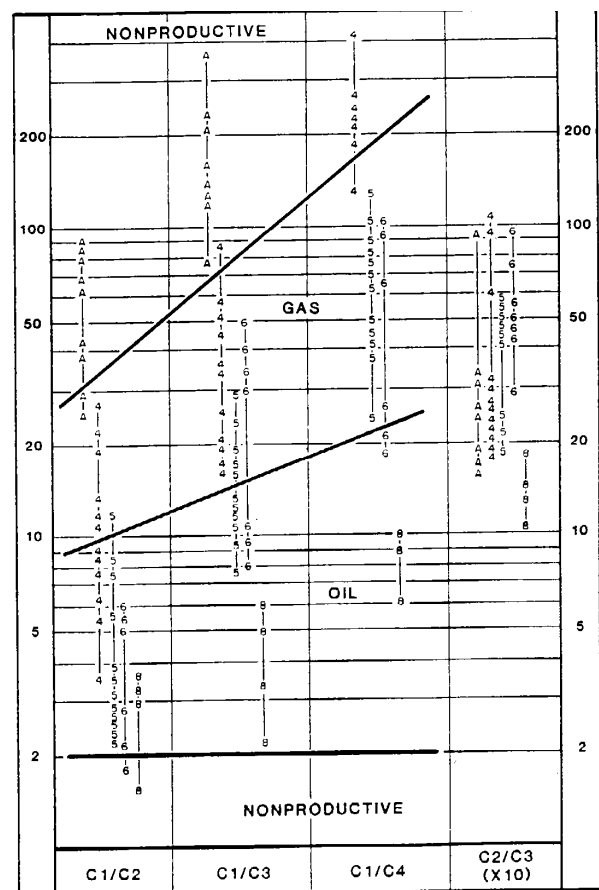| Relations Ⅱ	Oil zone	Gas zone	Other productive
C1/C2	2-10	10-35	< 2 and > 35
C1/C3	2-14	14-82	< 2 and > 82
C1/C4	2-21	21-200	< 2 and > 200

Fig. 1 Rectangular plot.

Fig. 2   Triangular Plot.

Fig. 3   Gas ratio method.
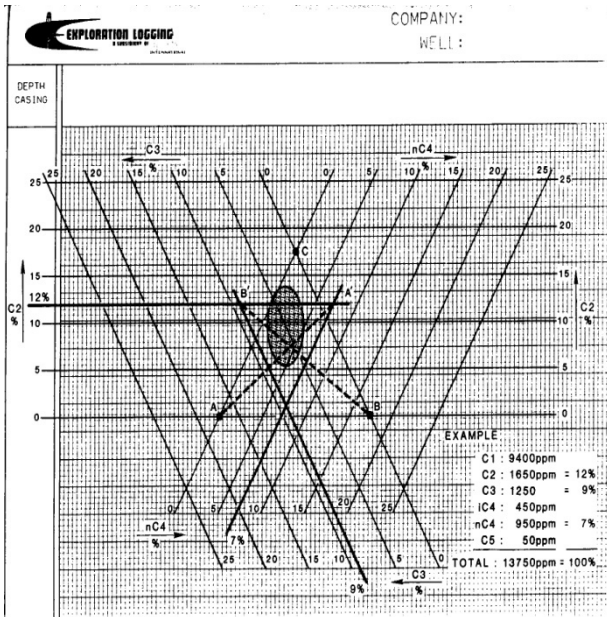
• If the apex of the triangle is up, gas is indicated—the smaller the up-apex triangle, the more water wet the gas.

• If the apex is down, oil is indicated—the larger the down-apex triangle, the heavier the oil.

• If the intersection of the lines between B to B' and A to A' occurs within the plotted ellipse, the zone is considered to be productive.

2.4 Gas Ratio Method

Gas ratio method (see Fig. 3) is a combination of three ratios, which when plotted together suggests a fluid character. The ratios are designed to be plotted on a depth log (unlike the Rectangular and Triangular plots) and still provide interpretative results. They were designed for ditch gas values rather than steam-still or DST values. The following ratios are used:

Hydrocarbon Wetness Ratio (Wh): when this parameter $\dfrac{C_2 + C_3 + C_4 + C_5}{C_1 + C_2 + C_3 + C_4 + C_5} \times 100$ is plotted (Table 2) it will increase with an increase in both gas and oil densities. Guidelines for the interpretation are:

Hydrocarbon Balance Ratio (Bh): this parameter $\dfrac{C_1 + C_2}{C_3 + C_4 + C_5}$ is related to the density of the reservoir fluid, decreasing with an increase in fluid density.

Hydrocarbon Character Ratio (Ch): this parameter $\dfrac{C_4 + C_5}{C_3}$ is used when excessive methane is present, which tends to retard the Wh and Bh ratios, affecting their curve movement. The Ch can also be used as a check and will aid in determining whether gas, oil or condensate potential is indicated.

Table 2   Witness ratio relations.
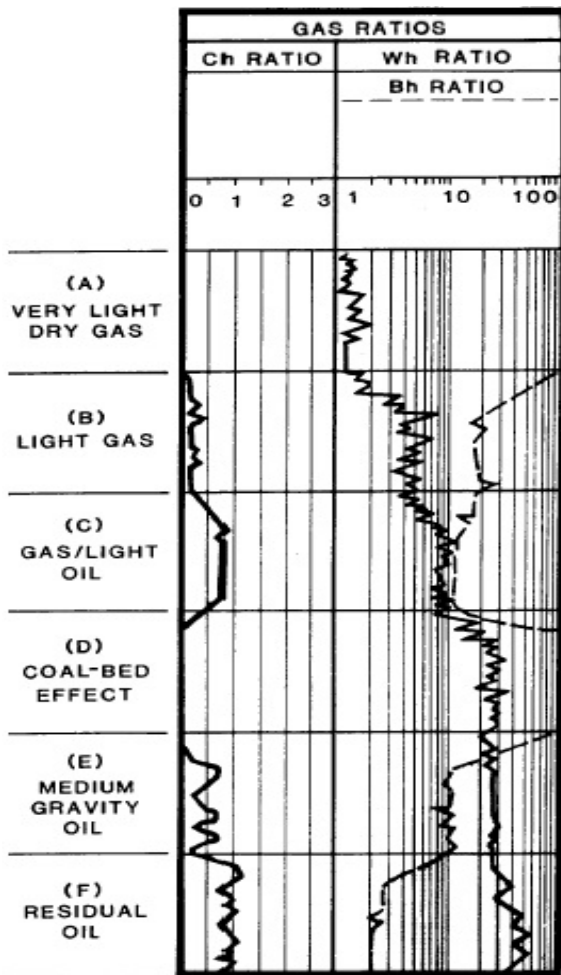
Wh (%)	Fluid potential
< 0.5	Non-productive dry gas
0.5-17.5	Potential gas–Increasing density with increasing Wh (%)
17.5-40	Potential oil–Increasing density with increasing Wh (%)
> 40	Residual oil

The interpretation of these ratios is a study of the relationships of the Wh, Bh and Ch curves and values. The first step is the study of the Wh, using the previously mentioned setpoints to determine the fluid character. Secondly, comparing the relationship of the Bh to the Wh will assist in confirming the fluid character in the following manner:

If the Bh is > 100, the zone is excessively dry gas;

If the Wh is in the gas phase and the Bh > Wh, the closer, the values/curves and the denser the gas;

If the Wh is in the gas phase and the Bh < Wh, gas/oil or gas/condensate is indicated;

If the Wh is in the oil phase and the Bh < Wh, the greater the difference/separation, the denser the oil;

If the Wh is in the residual oil phase and Bh < Wh, residual oil is indicated.

After comparing the Wh and Bh values/curves, the Ch is checked if situation 2 or 3 occur:

If the Ch < 0.5, gas potential is indicated and the Wh vs. Bh interpretation is correct;

If the Ch > 0.5, gas/light oil or condensate is indicated.

We can see these methods in below table and figures (Table 3, Fig. 4) which has been in Hovsan oil field

Table 3   Result of interpretation.

Oil-gas-condensate indicates								If BH > 100 excessive dry gas	Depth (m)	if CH < 0.5 wh and BH interpretation is correct	Depth (m)	If CH > 0.5 gas/light oil or condensate indicated	Depth (m)
Dry gas If wh < 0.5	Depth (m)	Potential gas wh-0.5 to 17.5	Depth (m)	Potential oil wh-17.5 to 40	Depth (m)	Residual oil Wh > 40	Depth (m)						
If BH > WH denser gas If BH < WH gas/oil or gas/condensate	Has not has not		has not	If BH < WH the denser the oil	3,933-3,937 3,941-3,958 4,093-4,119 4,191-4,201 4,215-4,222 4,259-4,262	If BH < WH the residual oil	2,031-3,933 9,37-3,941 3,958-4,093 4,119-4,191 4,201-4,215 4,222-4,259 4,262-4,296	Has not		Very little		2,031-4,296	

1. 3,933-3,937 m, 3,941-3,958 m, 4,093-4,119 m, 4,191-4,201 m, 4,215-4,222 m and 4,259-4,262 m intervals have denser oil.
2. 2,031-3,933 m, 3,937-3,941 m, 3,958-4,093 m, 4,119-4,191 m, 4,201-4,215 m, 4,222-4,259 m and 4,262-4,296 m intervals have residual oil.
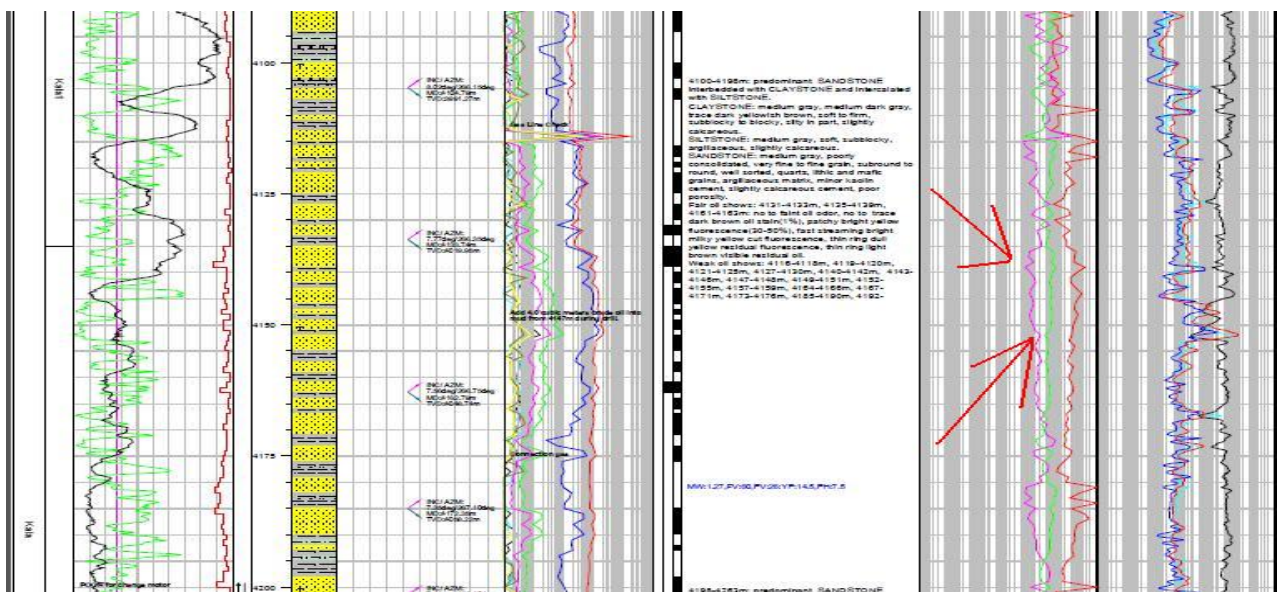

Fig. 4   Gas ratio curves in composite Log.

3. Result and Discussion

According above methods Samir Hashimov has made Table 3 who study Azerbaijan State Oil Academy.

Table 3 now is using in Surachani district, AOC company and using Qaradagh district, Pirsaat Hong Kong Company area. After we make full Table 3, we can say that on the oil well which zone have oil and which zone has gas. After comparison this method with wireline and mudlogging job it has been same result.

4.Conclusion

It means that this method help wireline team that make good desicion about perforation. In Azerbaijan I use gas ratio methods under composite log name. If we can look picture we can see wireline datas, oil layers, lithology, total gas, another gases and finally we can see modern gas analyses methods. When we compare those parameters, oil layers with modern methods (wh, bh and ch) this time we can see that those parameters and modern methods are the same and this show to us that which layer have oil and gas in the oil wells.

References

[1] Baker Hughes INTEQ. 1996. *Wellsite Geology-Reference Guide*. Houston: Baker Hughes INTEQ.
[2] Khalifazdeh, Ch. 1982. *Materials of lithology*, Azerbaijan Government Publisher.

Calibration of Hydrological Streamflow Modeling Using MODIS

Manithaphone Mahaxay[1], Wanchai Arunpraparut[2], Yongyut Trisurat[3] and Nipon Tangtham[4]

1.Watershed and Environmental Management Division, Department of Conservation, Kasetsart University, Bangkok 10900, Thailand

2. Department of Forest Engineering, Kasetsart University, Bangkok 10900, Thailand

3. Department of Forest Biology, Kasetsart University, Bangkok 10900, Thailand

4. Forest Research Center, Kasetsart University, Bangkok 10900, Thailand

Abstract: LULC (land use and land cover) plays an important role in mathematical hydrological modeling. As many countries, available LULC are not always updated to reflect the most current situation. In this regard, the objective of this study was to investigate the potential capability of moderate resolution satellite imagery such as MODIS (Moderate Resolution Imaging Spectroradiometer), acquired in 2010 for updated LULC. This issue was illustrated through the application of the most current LULC as one of the data inputs of the SWAT (Soil and Water Assessment Tool) model in the Tonle Sap Lake Basin, a sub-basin of the Mekong River. The streamflow was tested using moderate resolution LULC of 500 meters. The statistical evaluation results at a monitoring station for model calibration and validation showed that the R^2 for daily and monthly values range from 0.76 to 0.88 and 0.86 to 0.89 respectively, whereas the Nash-Sutcliffe efficiency daily and monthly values range between 0.75 to 0.85 and 0.76 to 0.87 respectively. The simulation result based on MODIS imagery demonstrates LULC at moderate resolution holds considerable potential as an effective hydrological modeling tool. An additional level of confidence is provided by the notion that the methods described here could be applied in similar watershed conditions.

Key words: LULC (land use and land cover), MODIS, SWAT (Soil and Water Assessment Tool), modeling, streamflow.

1. Introduction

LULC (land use and land cover) dataset, which is important in a watershed for hydrological and environmental modeling, require accurate LULC datasets to parameterize the physical system being simulated [1]. It is important that land-cover data be based on the most current data available, since the land-cover changes over time [2]. In watersheds, where LULC change takes place over the modeling period, using a single land-use geospatial data is not a true representation of the watershed condition [3]. The LULC data are one of the essential inputs for SWAT (Soil and Water Assessment Tool) model to which this research was applied.

SWAT is considered one of the most suitable physically-based models for simulating hydrological condition and is one of the most widely used watershed-scale water-quality models in the world. Nearly 600 peer-reviewed SWAT-related journal articles have been published and hundreds more have been published in conference proceedings and other formats [4]. Rossi et al. [5] pointed out that SWAT can potentially be used as an effective water quantity tool within Mekong basin. In which, SWAT model has been setup to simulate streamflow in each Mekong sub-basin [6]. In the Mekong Sub-basin the SWAT model has been calibrated using the most up-to-date available land use data of 2003 generated from Landsat image against available streamflow data for the period 1985-2000 [7]. The SWAT simulation result provided daily estimates of flow for 138 sub-basins covering

---

Corresponding author: Manithaphone Mahaxay, Ph.D., research fields: watershed management, remote sensing and GIS. E-mail: manithaphone@gmail.com.

entire the Lower Mekong basin except the delta south of Phnom Penh [6]. However, whether using simple or complex models, an accurate LULC dataset with an appropriate spatial or temporal resolution and level of detail is paramount for reliable predictions [8].

Landsat imagery is widely used to produce high resolution LULC data covering large river watershed. Although high resolution satellite imagery data can be extremely useful for LULC change detection and monitoring efforts, it can be difficult to obtain an image over the entire study area during a particular timeframe. In other words, only it is rarely possible to generate more than one scene of high resolution satellite imagery in a day. The revisit characteristics of the satellites, as well as the presence of cloud cover, can limit the availability of data [9]. In addition, spatial data, including land use, are usually expensive to obtain. This paper explores alternatives aimed at overcoming the limitations of LULC for hydrological modeling. To achieve the overall goal of the research, the status of LULC in 2010 was mapped out using both GIS (Geographic Information System) analysis and remote sensing data such as MODIS (Moderate Resolution Imaging Spectroradiometer) with 500 m resolution. The principle objective of this study is to assess whether free-data-MODIS can be effectively applied as an input for hydrological modeling. It is expected that the results of this study will contribute useful hydrologic information regarding the possibility of moderate-resolution of LULC data for large river watershed assessments.

2. Study Area

Tonle Sap Lake Basin is located in the northwest of Cambodia, between approximately latitudes 102° 15' to 105° 50'E and longitudes 11° 40' to 14° 28'N. The Tonle Sap Lake Basin is a sub-catchment of the Mekong basin. The total drainage area of Tonle Sap Lake Basin is approximately 85,786 km^2, including a permanent lake area of around 2,350 km^2. That is approximately 10.8% of the total area of the Mekong

basin [10]. The majority of the catchment is located in Cambodia and only 5% is in Thailand (Fig. 1). Ground altitudes range from 1 m to 1,500 m above sea level. About one third of the area is covered by forests that consist of a mixture of deciduous trees. There are agricultural areas and numerous small settlements as well.
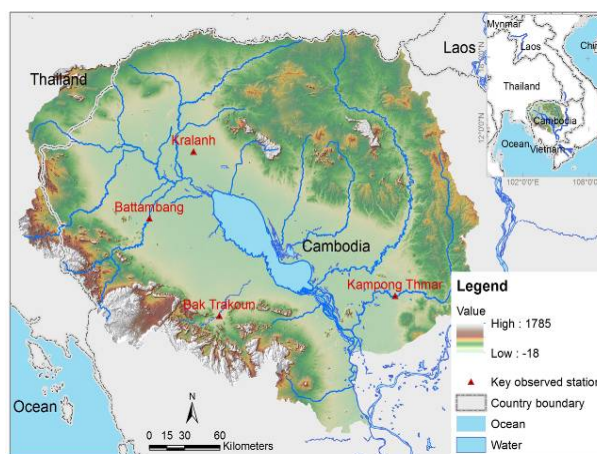

Fig. 1   Tonle Sap watershed.

3. Materials and Methods

3.1 Materials

Time series of 16-day composite MODIS imagery of MOD09A1 with 500 m resolution was acquired for LULC classification and mapping of spatial LULC of 2010. The other spatial data used are soil map of 50 m resolution based on FAO\UNESCO [11] classification system up to level three category and DEM (Digital Elevation Model)data of 50 m resolution. The other hydro-climatological quantities have been used from available gauges over the study area. Fig. 2 shows sets of required spatial data for SWAT hydrological modeling.

Most of the data preparation and analysis in this research was carried out using ArcGIS 10.1. Some specific image processing operations were executed using the ERDAS (Earth Resource Data Analysis System) Imagine software Version 8.0 (ERDAS Imagine is a remote sensing application designed for geospatial applications).
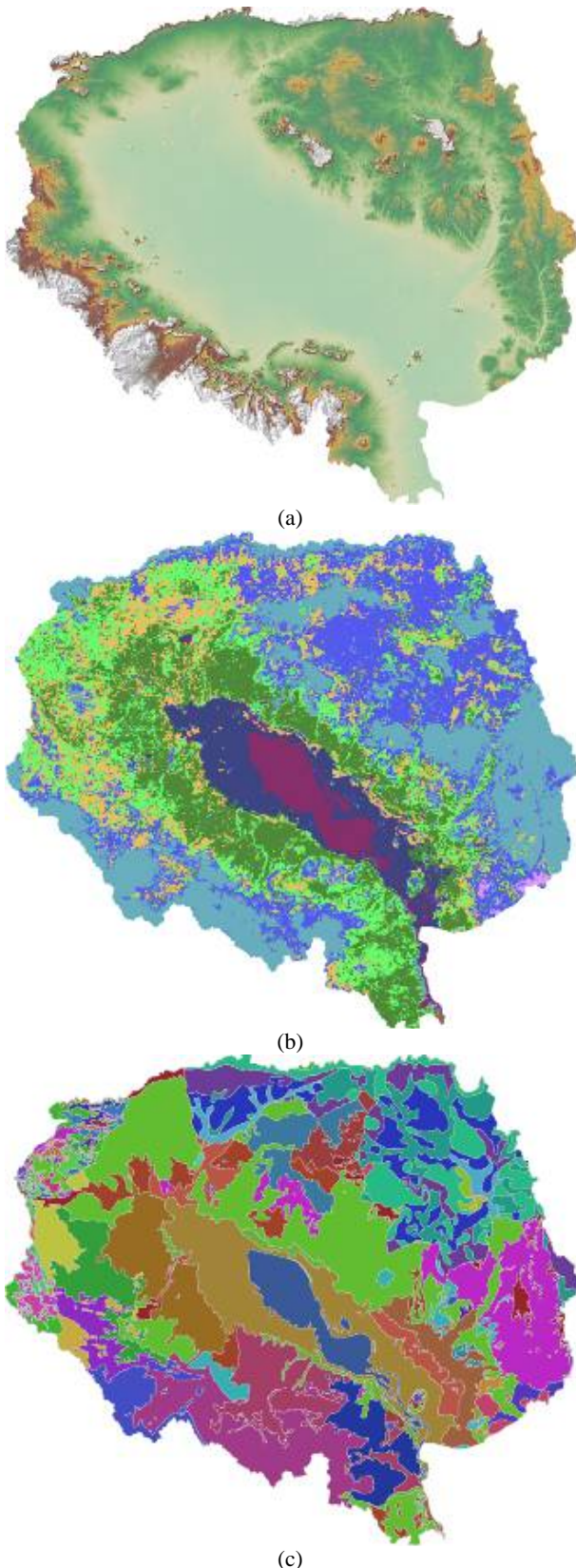
(a)

(b)

(c)

Fig. 2 Spatial data for SWAT model input: (a) DEM; (b) Land use; (c) Soil.

Other types of software employed are ArcSWAT Version 2012.10_1.7 for streamflow modeling and MRT (MODIS Reprojection Tool) for MODIS reprojection and transformation.

3.2 Methods

SWAT is a model developed by the USDA-ARS (United States Department for Agriculture, Agricultural Research Service). The main components of SWAT include hydrology, weather, sedimentation, soil temperature, crop growth, nutrients, pesticides and agricultural management. The model can be used to predict impacts of land management practices on water, sediment and agricultural chemicals in catchments [12, 13]. The SWAT model simulates hydrology as a two-component system, composed of land hydrology and channel hydrology. The land portion of the hydrologic cycle is based on a water mass balance. Soil water balance is the primary consideration by the model in each HRU (hydrological response unit), which Arnold et al. [14] represent as follow:

$$SW_t = SW + \sum_{i=1}^{t} (R_i - Q_i - ET_i - P_i - QR_i) \,(1)$$

where, *SW* is the soil water content; *i* is time in days for the simulation period *t*; and *R*, *Q*, *ET*, *P* and *QR* respectively are the daily precipitation, runoff, evapotranspiration, percolation and return flow.

LULC data used for this hydrological modeling were derived from satellite MODIS imagery. The LULC classification of 2010 LULC was carried out using supervised classification and every training site was carefully selected. Post-classification was performed based on existing land use map of 2003 generated from Landsat, DEM and ground survey. Accuracy assessment was also executed based on those field surveys and existing land use data. Overall classification accuracy was greater than 80% [15]. To make LULC data useable for SWAT, ArcSWAT interface requires a table linking the values represented to LULC types already defined in the model. Hence, the look-up table that converts the

LULC classification codes to SWAT land cover/plant codes was created manually in "ASCII.txt" format. Table 1 represents a look-up table for LULC categories conversion.

Table 1   Look-up table for the land use database use in SWAT.

Land use and land cover class		Land use class No.	SWAT database
Forest land	Evergreen	1	FRSE
	Deciduous	2	FRSD
	Plantation	3	PLAN
	Shrubland	4	SHRB
Crop land	Upland	5	AGRL
	Lowland paddy	6	PDDY
Others	Wetland	7	WETL
	Built-up land	8	URBN
	Water (rivers, lakes)	9	WATR

The soil units were also translated into SWAT user soil database. ArcSWAT creates the hydrologicresponse unit by combining DEM (Digital Elevation Model), soil and slope. Once DEM, land use and land cover, and soil data have been overlaid, the HRUs (hydrological Response Units) were generated. Rainfall data from 31 stations with time-series data from 1980 to 2008 were used as input data in SWAT. Additional rainfall data related to 2009 and 2010 were compensated by Global Weather Data for SWAT athttp://globalweather.tamu.edu/.

When all inputs were successfully entered, simulation was activated. Sensitivity analysis was carried out for help in determining the sensitivity of parameters by comparing variances in output caused by variability in the inputs. It also facilitates the selection of important and influential parameters for a model calibration by indicating the parameters that display higher sensitivity in output due to input variability. Streamflow simulations were calibrated using LULC in 2010. Overall procedure of SWAT application in this research is shown in Fig. 3.
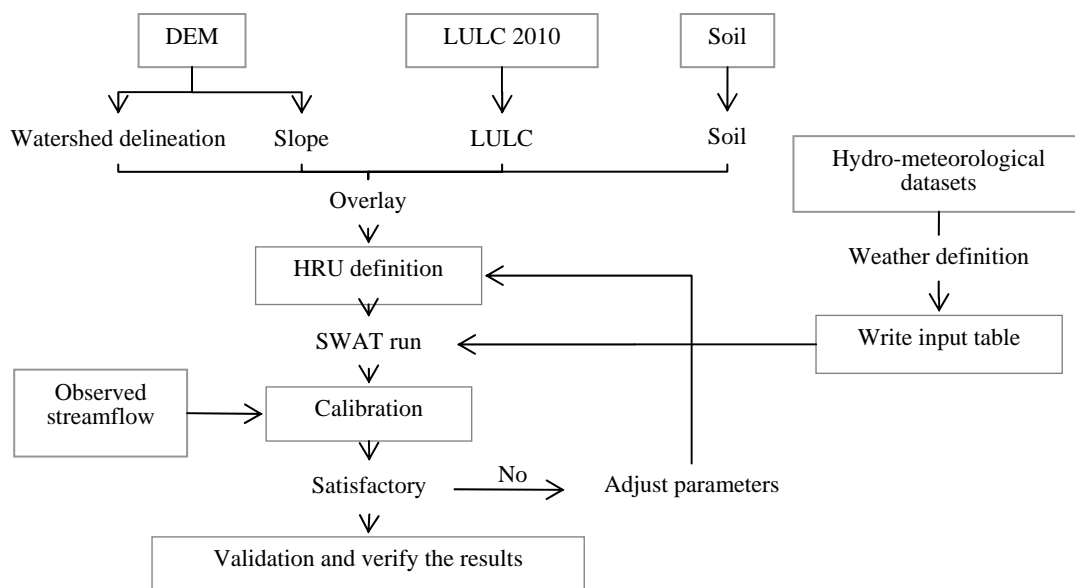

Fig. 3   Flow chart of streamflow modeling process.

The streamflow was run at the outlet of selected hydrological stations at daily and monthly time steps for the period January through December 2010. Calibration was performed on the 1997 to 2009 years, while the years from 1980 to 1996 were used for model warm-up period. To verify the results, the performance of the model in simulating streamflow was evaluated using *ENS* or *NSE* or E_{NS} (Nash–Sutcliffe efficiency) and the coefficient of determination (R^2) [16]. The Nash-Sutcliffe statistic is a measure of how well the observed variance is simulated [17]. The equations used were as follows:

$$E_{NS} = 1 - \frac{\sum_{i=1}^{n}(O_i - P_i)^2}{\sum_{i=1}^{n}(O_i - \bar{O})^2} \qquad (2)$$

where, O_i and P_i are the observed and simulated data, respectively; $\bar{O}$ is the average of the observed data and n is the total number of data records.

$$R^2 = 1 - \frac{\sum(Y_i - \hat{Y}_i)^2}{\sum(Y_i - \bar{Y})^2} \qquad (3)$$

where, Y_i denotes the value of the ith dependent variable, $\bar{Y}$ is the mean of the dependent variable and $\hat{Y}_i$ is the ith fitted value.

4. Results and Discussion

4.1 Sensitivity Analysis

Sensitivity analysis has been carried out for each available observed streamflow data of each LULC SWAT project. SUFI2 (Sequential Uncertainty Fitting)

for the calibration of uncertainty in procedure was used for this analysis. Five parameters were found to be sensitive, with relative sensitive values in the range of 0.031 to 0.034. The most sensitive parameters are threshold depths of water in the shallow aquifer for "revap" to occur (REVAPMN.gw), Alpha_Bf factor (base flow alpha), Gw_Revap coefficient (groundwater "revap"), ESCO factor (soil evaporation compensation), initial SCS CN2 value (Curve Number II) respectively. These sensitive parameters were considered for model calibration. The remaining parameters had no significant effect on streamflow simulations. Changes in their values do not cause significant changes in the model output.

4.2 Calibration and Validation for Streamflow Estimation

Hydrological streamflow results for the observation station at Kampong Thmar gauge is being discussed (Fig. 4).
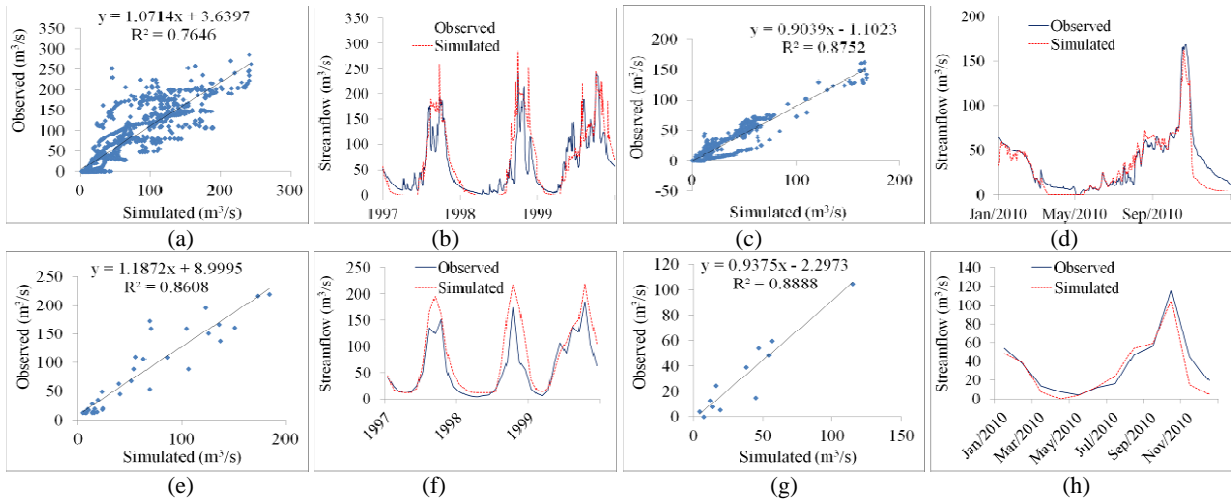

Fig. 4 Simulation results: (a) and (b)—Daily calibration result; (c) and (d)—Monthly calibration result; (e) and (f)—Daily validation result; (g) and (h)—Monthly validation result.

The monthly calibration results have shown better agreement between monthly observed and simulated flows in both calibration and validation processes. The result of the E_{NS} and R^2 are as high as 0.88 and 0.89 respectively (Table 2). Based on the statistical analysis of model evaluation results, conclusion of whether MODIS can be effectively applied as an input to

SWAT interface for hydrological streamflow modeling is noticeable.

Table 2 Calibration and validation results.

	Calibration		Validation	
	E_{NS}	R^2	E_{NS}	R^2
Daily	0.75	0.76	0.85	0.88
Monthly	0.76	0.86	0.87	0.89

However, according to Benaman et al. [18], model simulation can be judged as satisfactory if R^2 is greater than 0.6 and E_{NS} is greater than 0.5. Hence study results agree reasonably well with these accuracy simulations of LULC parameters. Some of the model inaccuracy are caused due to data gaps and lack of accurate and efficient input data where is available such as rainfall, temperature and evapotranspiration. Hence, to increase model efficiency it is obviously depending on such data inputs, as well suitable distribution of the measuring stations over the watershed is required.

5. Conclusions

Model produced good simulation results for daily time steps which have demonstrated that moderate resolution of non-commercial and freely-available satellite imagery like MODIS holds considerable potential for application in hydrological modeling. However, the use of other hydrological models would be more beneficial for the hydrological modeler in order to enhance our understanding of alternative MODIS-based LULC as an input parameter for hydrological modeling. In addition to the modeling tool, the assessment of LULC data input capability would be more beneficial if simulation is tested by a number of hydrological parameters other than streamflow, such as surface run-off, water quality, etc.

Acknowledgment

References

[1] Burian, S., Brown, M., and McPherson, T. 2002. "Evaluation of Land Use and Land Cover Datasets for Urban Watershed Modeling." *Water Science and Technology* 45 (9): 269-76.

[2] Chen, P., Luzio, M. D., and Arnold., J. G. 2005. "Impact of Two Land-cover Data Sets on Streamflow and Total Nitrogen Simulations Using A Spatially Distributed Hydrologic Model." Presented at the ASPRS 2005—Pecora 16 "Global Priorities in Land Remote Sensing" Sioux Falls, South Dakota, USA.

[3] Pai, N., and Saraswat, D. 2011. "SWAT2009_LUC: A Tool to Activate the Land Use Change Module in SWAT 2009." *Transactions of the American Society of Agricultural and Biological Engineers* 54 (5): 1649-58.

[4] Gassman, P. W., Arnold, J., Srinivasan R., and Reyes, M. 2010. "The Worldwide Use of the SWAT Model, Technological Drivers, Networking Impacts, and Simulation Trends." Presented at the 21st Century Watershed Technology, Improving Water Quality and Environment Conference Proceedings, Universidad EARTH, Mercedes, Costa Rica.

[5] Rossi, C. G., Srinivasan, R., Jirayoot, K., Duc, T. L., Souvannabouth, P., Bin, N., and Gassman, P. W. 2009. "Hydrological Evaluation of the Lower Mekong River Basin with the Soil and Water Assessment Tool Model." *International Agricultural Engineering Journal* (18): 1-13.

[6] Mainuddin, M., Hoanh, C. T., Jirayoot, K., Halls, A. S., Kirby, M., Lacombe, G., and Srinetr, V. 2010. "Adaptation Options to Reduce the Vulnerability of Mekong Water Resources, Food Security and the Environment to Impacts of Development and Climate Change." *CSIRO, Water for a Healthy Country National Research Flagship*: 152.

[7] Johnston, R., Rowcroft, P., Hortle K. G., and McAlister, C. 2003. "Hydrological Models of the Lower Mekong Basin at MRC." Presented at the Workshop on Integrating Environmental Impacts into Water Allocation Models of the Mekong River Basin, University of Economics, Ho Chi Minh City, Vietnam.

[8] Huang, J., Zhou, P., Zhou. Z., and Huang, Y. 2013. "Assessing the Influence of Land Use and Land Cover Datasets with Different Points in Time and Levels of Detail on Watershed Modeling in the North River Watershed, China." *International Journal of Environmental Research and Public Health* (10): 1660-4601.

[9] WRP (Wetlands Research Program). 1994. The Corps of WRP (Wetlands Research Program). 2004. "Remote Sensed Data, Information for Monitoring Dynamic Wetland Systems." Remote Sensing/GIS Support Center, U.S. Army Cold Regions Research and Engineering Center. Accessed Nov 1, 2013. http://el.erdc.usace.army.mil/elpubs/pdf/wgsw2-1.pdf.

[10] MRC (Mekong River Commission). 2003. *State of the Basin Report.* Executive summary.

[11] FAO. 1988. FAO/UNESCO Soil Map of the World, Revised Legend, with Corrections and Updates. World soil resources report 60, FAO, Rome.

[12] Neitsch, S. L., Arnold, J. G., Kiniry, J. R., and Williams, J. R. 2009. *Soil and Water Assessment Tool.* Theoretical Documentation, Version 2000. Texas, USA: USDA Agricultural Research Service and Texas A & M Blackland Research Center.

[13] Chaplot, V., Saleh, A., and Jaynes, D. B. 2004. "Predicting Water, Sediment and NO_3–N Loads under Scenarios of Land-Use and Management Practices in a Flat Watershed." *Water, Air, & Soil Pollution* (154): 271-93.

[14] Arnold, J. G., Srinivasan, P., and Muttiah, R. S. 1998. "Large Area Hydrologic Modeling and Assessment. Part I. Model Development." *The Journal of the American Water Resources Association (JAWRA)* 34: 73-89.

[15] Mahaxay, M. 2014. "Evaluation of MODIS Through Its Application in Land Use and Land Cover Change Effect on Streamflow: Tonle Sap Basin, Cambodia." Ph.D. thesis, Kasetsart University.

[16] Eisenhauer, J. G. 2003. "Regression through the Origin."*Teaching Statistics* 25 (3):76-80.

[17] Nash, J. E., and Sutcliffe, J. 1970. "River Flow Forecasting through Conceptual Models. Part I—A Discussion of Principles."*Journal of Hydrology* 10 (3): 282-90.

[18] Benaman, J., Christine, A. S., and Douglas, A. H. 2005. "Calibration and Validation of Soil and Water Assessment Tool on An Agricultural Watershed in Upstate New York." *Journal of Hydrologic Engineering* 10 (5): 363-74.